GEORGIA INSTITUTE OF TECHNOLOGY — OFFICE OF CONTRACT ADMINISTRATION

PROJECT ADMINISTRATION DATA SHEET

[X] ORIGINAL [ ] REVISION NO. _____

Project No. A-3326 — DATE 8/20/82

Project Director: ~~Dr. G. R. Loefer~~ Dr. A MULLIKIN MISC — School/Lab EML

Sponsor: National Research Laboratory

Washington, DC 20375 81-K-2016

Type Agreement: SFRC No. N00014-~~82-K-2016~~; Mod. P00002

Award Period: From 5/20/82 To ~~6/20/83~~ 11/20/83 (Performance) 8/20/83 (Reports)

Sponsor Amount: $71,535 — Contracted through:

Cost Sharing: N/A — GTRI/~~GIT~~

Title: Conscan Seeker Model Study

ADMINISTRATIVE DATA

OCA Contact Linda H. Bowman X4820

1) Sponsor Technical Contact:

Dr. F. R. Barone, Scientific
Program Officer; Attn: Code 6552
N-R-L
Washington, D.C. 20375

2) Sponsor Admin/Contractual Matters:

ONR RR
Campus

(404) 881-4213

Defense Priority Rating: N/A

Security Classification: unclassified

RESTRICTIONS

See Attached Gov't Supplemental Information Sheet for Additional Requirements.

Travel: Foreign travel must have prior approval – Contact OCA in each case. Domestic travel requires sponsor approval where total will exceed greater of $500 or 125% of approved proposal budget category.

Equipment: Title vests with GIT if specified in the proposal and not otherwise indicated in the Short Form Research Contract

COMMENTS:

Continuation of A-2991

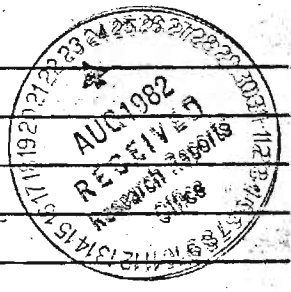

COPIES TO: Research Administrative Network

~~Administrative Coordinator~~
Research Property Management
Accounting
Procurement/EES Supply Services
Research Security Services
~~Reports Coordinator (OCA)~~
Legal Services (OCA)
Library
EES Public Relations (2)
Computer Input
Project File
Other _____

FORM OCA 4:781

B108 T2345

GEORGIA INSTITUTE OF TECHNOLOGY

OFFICE OF CONTRACT ADMINISTRATION

SPONSORED PROJECT TERMINATION/CLOSEOUT SHEET

Date February 20, 1984

Project No. A-3326

~~School~~ Lab EML

Includes Subproject No.(s) ----

Project Director(s) Dr. A.L. Mullikin

Sponsor National Research Laboratory

Title Conscan Seeker Model Study

Effective Completion Date: 11/20/83

Grant/Contract Closeout Actions Remaining:

- [ ] None
- [x] Final Invoice or ~~Final Fiscal Report~~
- [x] Closing Documents
- [x] Final Report of Inventions
- [x] Govt. Property Inventory & Related
- [ ] Classified Material Certificate
- [ ] Other

Continues Project No. A-2991

COPIES TO:

Project Director
Research Administrative Network
Research Property Management
Accounting
Procurement/EES Supply Services
~~Research Security Services~~
Reports Coordinator (OCA)
Legal Services

Form OCA 60:1028

THE NATIONAL LIBRARY BINDERY CO.
2395 PEACHTREE ROAD, N. E. ATLANTA, GEORGIA 30305

BUCKRAM (Specify Color by number) C2

"Please Check"

Covers	In	☑
	Out	☐
Index	Front	☐
	Back	☐
Ads	In	☐
	Out	☐
Bind Regular Way		☐
Bind Intact		☐
Bind Imperfect		☐
Sample Sent		☐
*Rub on File (at Bindery)		☐
*Keep A Rub (at Bindery)		☐
1st Time Bound By Nat'l		☐
Do Not Trim Edges		☐

Lettering:

Follow Old Spine	☐
Cross Spine	☑
On Front	☐
Lengthwise	☐
Gold	☑
Black	☐
White	☐
Insert Stubs For Missing Pages	☐
*Pattern	

ARRANGE LETTERING AS DESIRED ON SPINE

Mullikin—
Conscan
Seeker
Model/
Study

N-B+T

B108 336

2-

Send two copies of binding slip with volume.
Original slip must accompany volume returned for correction.

F-3-1034

FINAL REPORT
GT/EES Project No. A-3326

MODIFICATIONS TO DISAMS-1
(Digital Infrared Surface to Air Missile Simulation)

By
A. L. Mullikin

Prepared for
NAVAL RESEARCH LABORATORY
Dr. Frank Barone
Code 6552
Washington, D.C. 20375

Under
NRL Contract #N00014-82-K-2016

January 1984

GEORGIA INSTITUTE OF TECHNOLOGY
A Unit of the University System of Georgia
Engineering Experiment Station
Atlanta, Georgia 30332

1984

UNCLASSIFIED

SECURITY CLASSIFICATION OF THIS PAGE *(When Data Entered)*

REPORT DOCUMENTATION PAGE		READ INSTRUCTIONS BEFORE COMPLETING FORM
1. REPORT NUMBER A-3326	2. GOVT ACCESSION NO.	3. RECIPIENT'S CATALOG NUMBER
4. TITLE *(and Subtitle)* MODIFICATIONS TO DISAMS-1 (DIGITAL INFRARED SURFACE TO AIR MISSILE SIMULATION)		5. TYPE OF REPORT & PERIOD COVERED FINAL REPORT 6. PERFORMING ORG. REPORT NUMBER A-3326
7. AUTHOR(s) A. L. MULLIKIN		8. CONTRACT OR GRANT NUMBER(s) N00014-82-K-2016
9. PERFORMING ORGANIZATION NAME AND ADDRESS GEORGIA INSTITUTE OF TECHNOLOGY ENGINEERING EXPERIMENT STATION ATLANTA, GA 30332		10. PROGRAM ELEMENT, PROJECT, TASK AREA & WORK UNIT NUMBERS
11. CONTROLLING OFFICE NAME AND ADDRESS NAVAL RESEARCH LABORATORY WASHINGTON, DC 20375		12. REPORT DATE JANUARY, 1984 13. NUMBER OF PAGES 75
14. MONITORING AGENCY NAME & ADDRESS*(if different from Controlling Office)*		15. SECURITY CLASS. *(of this report)* UNCLASSIFIED 15a. DECLASSIFICATION/DOWNGRADING SCHEDULE
16. DISTRIBUTION STATEMENT *(of this Report)*		
17. DISTRIBUTION STATEMENT *(of the abstract entered in Block 20, if different from Report)*		
18. SUPPLEMENTARY NOTES		
19. KEY WORDS *(Continue on reverse side if necessary and identify by block number)* Digital Modeling Infrared Countermeasures Evaluation Infrared Seeker Evaluation Seeker Modeling Terminal Homing 6-DOF Model		
20. ABSTRACT *(Continue on reverse side if necessary and identify by block number)* Several modifications and additions have been made to the DISAMS-1 6-DOF model developed at Georgia Tech, the most significant being the inclusion of a NWSC (Crane, Indiana) flare model. Validation of and footprints generated by the model are also presented.		

DD FORM 1 JAN 73 1473 EDITION OF 1 NOV 65 IS OBSOLETE

UNCLASSIFIED

SECURITY CLASSIFICATION OF THIS PAGE *(When Data Entered)*

FINAL REPORT A-3326

MODIFICATIONS TO DISAMS-1
(DIGITAL INFRARED SURFACE TO AIR MISSILE SIMULATION)

Prepared by
A. L. Mullikin

January 1984

NRL Contract #N00014-82-K-2016

Georgia Tech Project A-3326

For

Dr. Frank Barone
Code 6552
Naval Research Laboratory
Washington, D.C. 20375

TABLE OF CONTENTS

		List of Figures.	iv
		List of Tables.	vii
Section	1.0	Introduction.	1
	2.0	Initial Values.	2
	3.0	Modification of the "LNCH" parameter.	5
	4.0	The SUMRY File.	7
	5.0	The Flare Model.	10
	5.1	Input.	10
	5.2	Subroutine Communication and Calculation.	15
	5.3	Output.	18
	6.0	Model Validation.	26
	7.0	Footprint Predictions Using DISAMS-1	42
	8.0	Anomalies for Multiple Source Targets.	58

LIST OF FIGURES

Figure 2.0-1	Definition of the target crossing angle.	4
4.0-1	Example of a SUMRY output file.	9
5.1-1	Example of a FLRDAT input file.	20
5.3-1	A portion of a TXYZ output file.	25
6.0-1	Cable car positions.	30
6.0-2	Cable car velocities.	31
6.0-3	Measured and calculated positions for round #5.	32
6.0-4	Measured and calculated positions for round #6.	33
6.0-5	Measured and calculated positions for round #7.	34
6.0-6	Measured and calculated positions for round #8.	35
6.0-7	Measured and calculated positions summary.	36
6.0-8	Measured and calculated velocities for round #5.	37
6.0-9	Measured and calculated velocities for round #6.	38
6.0-10	Measured and calculated velocities for round #7.	39
6.0-11	Measured and calculated velocities for round #8.	40
6.0-12	Measured and calculated velocity summary.	41
7.0-1	Footprint for scenario #1.	45

LIST OF FIGURES (CONT.)

7.0-2	Footprint for scenario #2.	46
7.0-3	Footprint for scenario #3.	47
7.0-4	Footprint for scenario #4.	48
7.0-5	Footprint for scenario #5.	49
7.0-6	Footprint for scenario #6.	50
7.0-7	Footprint for scenario #7.	51
7.0-8	Footprint for scenario #8.	52
7.0-9	Footprint for scenario #9.	53
7.0-10	Footprint for scenario #10.	54
7.0-11	Footprint for scenario #11.	55
7.0-12	Footprint for scenario #12.	56
7.0-13	Footprint summary.	57
8.0-1	Source positions on the reticle at t = 0.	68
8.0-2	Detector output for source positions on Figure 8.0-1.	69
8.0-3	Detector signal and resulting seeker output.	69
8.0-4	Demodulator signal.	70
8.0-5	Image position geometry.	70
8.0-6	Two source target image positions.	71
8.0-7	Detector and seeker signals for positions A,B of Figure 8.0-6.	72
8.0-8	Source position - error signal relations.	73
8.0-9	Centroid relations.	73
8.0-10	Detector and seeker signals for positions C,D of Figure 8.0-6.	74

LIST OF FIGURES (CONT.)

8.0-11(a) Source positions on the reticle. 75
8.0-11(b) Phase change in the error signal. 76

LIST OF TABLES

Table 5.2-1(a)	Variables passed to or from FDECOY.	21
5.2-1(b)	Variables passed to or from FDECOY.	22
5.2-1(c)	Variables passed to or from FDECOY.	23
5.2-2	Variables passed to or from FLARE.	24
6.0-1	Parameters for live firings.	29
7.0-1	Scenario identification for Figures 7.0-1 through 7.0-12	44

1.0 Introduction

Since its original documentation in 1983, the DISAMS-1 program has been modified and expanded in several respects. Further efforts have been made to validate the model, particularly with respect to the interaction between the seeker and airframe models, and the model has been used in at least one instance to predict footprints for the missile. Much of this work has been reported in various documents of very limited distribution. To make it more accessible, it has all been included in this report.

The major change in DISAMS-1 is that a flare model, which was developed at NWSC, Crane, Indiana has been modified and included. In addition, some initialization procedures have been changed so that the model more nearly conforms to the hardware conventions. A new output file, TAPE27 = SUMRY, which contains a very short summary of the simulation is also now available. A number of other technical changes have been made, but these are essentially transparent to the user.

The changes and their impact on the user will be discussed in the following paragraphs. In this discussion, it is assumed that the reader is familiar with the documentation for the original model (1).

2.0 Initial Values

In the original DISAMS-1 model, the gyro angular tracking rates were initially zero even through the line of sight rates might not be. By alteration of and addition to some of the code in the SEEKER subroutine, that initialization has now been changed so that the initial gyro angular rates are the same as the LOS angular rates. No action is required of the user to effect this change.

Although provision was made in the original DISAMS-1 for the user to impose super elevation (E) and a lead angle (A) on the missile before launch, default values for these angles were zero. The user still has that option, and it is exercised exactly as before, but default initial values are now determined by the initial target missile geometry. In particular, the missile is always assigned a minimum elevation of 20°. Thus, if the actual initial missile to target elevation is THMB, E is defined by

$$E = 20^{\circ} - THMB \qquad THMB < 20^{\circ}$$
$$E = 0^{\circ} \qquad THMB > 20^{\circ}$$

This convention is overridden if E is assigned a nonzero value by the user. In either event, the value of E used in the simulation is printed on the TAPE6 = OUTPUT file in the list of parameter values.

The default definition of A is more complicated.

Let TCA be the "crossing angle" as defined by Figure 2.0-1 and define A, in degrees, by

$$A = 10\sqrt{2}\,\sin(TCA) \qquad \sin(TCA) < 1/\sqrt{2}$$
$$A = 10 \qquad \sin(TCA) \geq 1/\sqrt{2}$$

This provides up to 10^{o} of lead. Again, a nonzero value of A input by the user overrides this convention and the value of A used in the simulation is printed on the OUTPUT file in the list of parameter values.

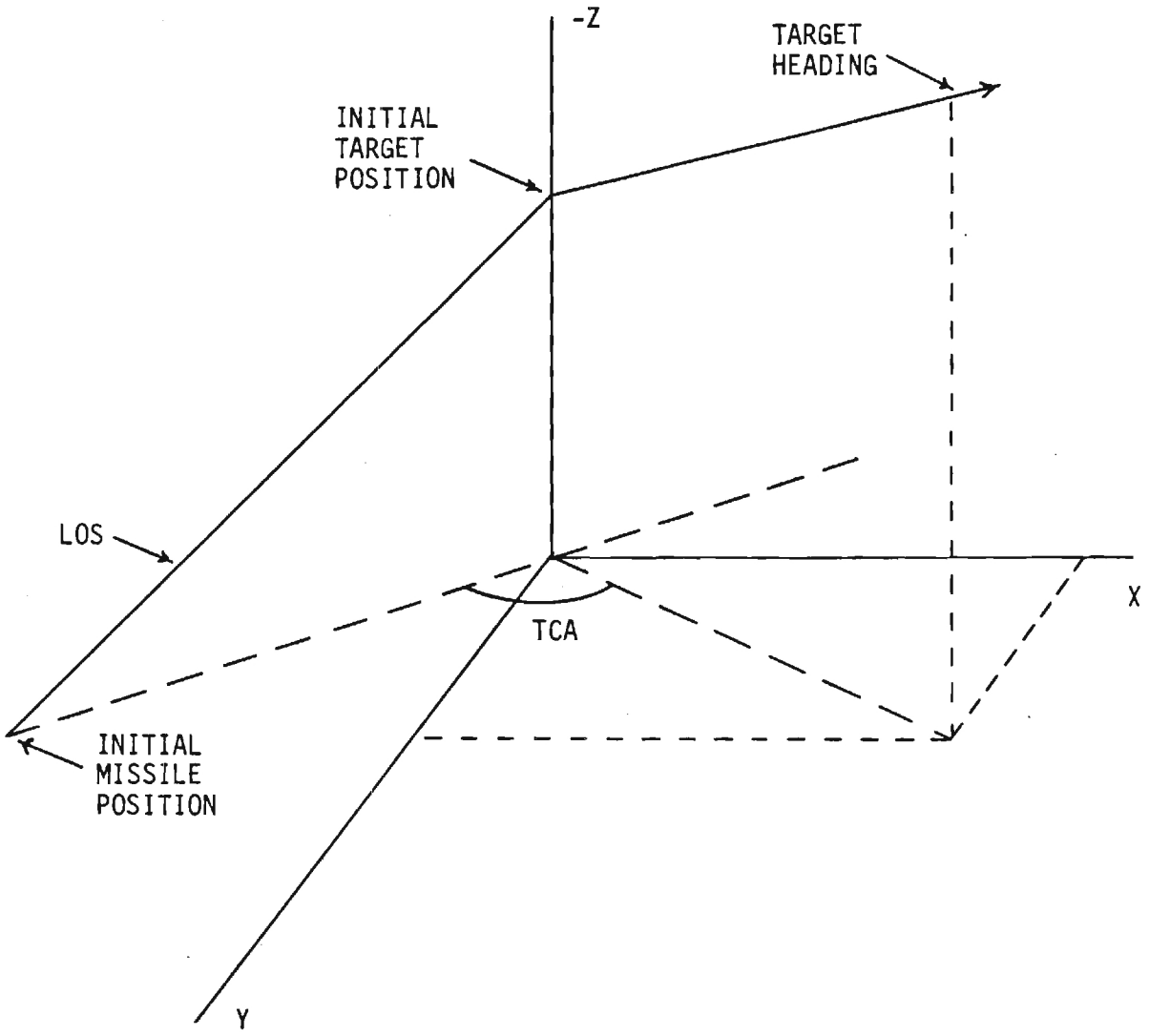

Figure 2.0-1 Definition of the target crossing angle TCA.

3.0 Modification of the "LNCH" Parameter

In DISAMS-1, if LNCH has its default value of one, the missile is launched at the beginning of the simulation regardless of target signal strength. If LNCH = 0, launch is delayed until the target signal generates sufficient missile audio for the seeker to track. In that mode, the seeker attitude during the prelaunch phase is determined solely by missile-target geometry. A new value for LNCH is now defined, LNCH = -1. In this mode, it is assumed that sufficient target strength is present for the seeker to track, but a launch is not made. Thus the model operates in a captive mode in that all target maneuver options are available to the user, but only seeker output will be calculated. Missile position and orientation are held at their initial values. If target motion is great, the gyro angular travel may cause the gyro to attain its angular limits. Meaningless output would then be generated for the remainder of the simulation. It is suggested that IBORT be set equal to 1 if LNCH = -1. This has the effect of stopping the simulation if gyro angular limits are attained. Note that the duration of the simulation normally will be determined by NUCYCL. However, if the missile to target distance decreases, then begins to increase as a result of the target flight path, the simulation will terminate. That action is a consequence of the algorithm used in the model to determine minimum missile to target distance, i.e., miss distance, and to terminate the

simulation when it is attained.

4.0 The SUMRY File

A greatly abbreviated summary file, TAPE27 = SUMRY, has been added to the list of files generated by the program. Each simulation generates four lines of data. These data are:

```
IRUN, T, DIST
XM0, YM0, ZM0, XT0, YT0, ZT0, VT
XMF, YMF, ZMF, XTF, YTF, ZTF,
RTMX, RTMY, RTMZ
```

where

IRUN	is the simulation identification number.
T	is the elapsed time of the simulation.
DIST	is the miss distance if less than 40.0, otherwise DIST = 9999.9.
XM0, YM0, ZM0	are the initial missile earth coordinates.
XT0, YT0, ZT0	are the initial target earth coordinates.
VT	is the initial target speed.
XMF, YMF, ZMF	are the final missile earth coordinates.
XTF, YTF, ZTF	are the final target earth coordinates.

RTMX, RTMY, RTMZ are the final missile to target vector earth components.

An example of this file is shown in Figure 4.0-1 for a run consisting of two simulations.

```
1050     6.890 9999.900
  -4000.0    4000.0       0.0       0.0       0.0  -3000.0     350.0
   2394.8    -282.3  -2631.7    2411.6       0.0  -3000.0
     16.9     282.2   -368.4
1051     4.890    1.113
  -3000.0       0.0       0.0       0.0       0.0  -3000.0     227.3
   1112.2       -.4  -2999.4    1111.3       0.0  -3000.0
      -.8        .4       -.7
```

Figure 4.0-1 Example of a SUMRY output file.

5.0 The Flare Model

Several subroutines have been added to DISAMS-1 to give the target the capacity to eject up to 50 identical flares at user selected time intervals, positions, and angles (relative to the launching platform). A new parameter NFLR has been introduced into the CNGPRM NAMELIST in DISAMS-1. For the default value NFLR = 0, the flare routines are not used, NFLR = 1 enables the flare option.

The flare model itself is essentially contained in the subroutine FLARE and the subroutines that it calls. A second subroutine, FDECOY, provides the interface between the flare model and DISAMS-1. The times and angles, relative to the launching platform, at which the flares are launched are controlled by FDECOY. Flare characteristics, intensity, aerodynamic data, position, etc., are managed by FLARE. These routines assume that the flares are identical and except for initial direction and position relative to the launching platform, are ejected by identical mechanisms. User control and flare characteristics are input to the program through the formatted file TAPE9 = FLRDAT. If NFLR = 1, this file is expected. A description of each line of this file follows.

5.1 Input

The first line of FLRDAT contains three integers.

KFLRT, LANGP, and LTIMP formatted by FORMAT(1X,3I3). KFLRT is the total number of flares available for the simulation ($1 \leq FLRT \leq 0$). Depending on the rate at which these flares are dispensed and the duration of the simulation, all of the flares may not be ejected.

The ejection angles and positions of the flares are controlled, in part, by LANGP. For each flare, two angles are required, azimuth (EBETA) and elevation (EALPHA) both in degrees. These angles are measured relative to the launching platform coordinate system as follows. Suppose the launching platform is an airplane. The positive x axis points out the nose, the positive y axis out the right wing, and, to complete a right handed system, the z axis points out the bottom of the aircraft. Azimuth, relative to this system, is positive when measured from the positive x axis to the positive y axis. Elevation is measured positive from the positive x axis to the negative z axis. The origin is at the center of gravity of the airplane. Launcher position, FLX0, FLY0, FLZ0, in launch platform coordinates, must also be given (in feet).

A different ejection set (EALPHA, EBETA, FLX0, FLY0, FLZ0) can be prescribed for each flare, or the flares can be launched periodically in the sense that flares numbered 1 through LANGP are ejected at prescribed angles and positions, remaining flares are ejected at repetitions of that sequence of angles and positions. This information is written on the file FLRDAT in the following format. After the line containing KFLRT, LANGP, and LTIMP should follow LANGP lines of the form

EALPHA, EBETA, FLX0, FLY0, FLZ0

using FORMAT(1X,5E10.3).

As an example, albeit an unrealistic one, suppose an aircraft has three flare dispensers, one on the right side, one on the left side, and one on the bottom. Suppose the coordinates of the launchers in the aircraft coordinate system are (0.0, 5.0, 3.0), (0.0, -5.0, 3.0), and (-10.0, 0.0, 5.0) respectively. The first flare is to be launched straight down, EALPHA = -90.0 EBETA = 0.0, from the bottom launcher; the next two from the right hand launcher straight out from the aircraft, EALPHA = 0.0, EBETA = 90.0; and the next, also from the left launcher, straight out but down 45°, EALPHA = -45.0, EBETA = -90.0. Lines 2-6 of FLRDAT would then be

-90.000	0.000	-10.000	0.000	5.000
0.000	90.000	0.000	5.000	3.000
0.000	90.000	0.000	5.000	3.000
0.000	-90.000	0.000	-5.000	3.000
-45.000	-90.000	0.000	-5.000	3.000

In this case LANGP = 5. If KFLRT is greater than five, the pattern established by these five lines will be repeated until all available flares, KFLRT, are expended. Note: KFLRT is not required to be a multiple of LANGP.

Prescription of ejection times is slightly more complicated. The first time value given, T1, is the ejection time in seconds of the first flare measured from the beginning of the simulation. The next value, T2, if there is one, is the time interval between ejec-

tion of the first flare and the second; the next time value T3, if there is one, is the time interval between ejection of the second flare and the third, etc. LTIMP (LTIMP > 0) is the number of these intervals that are given. Note that the number of time values given is then LTIMP + 1. If KFLRT is greater than LTIMP + 1, the time intervals are repeated. The time values are recorded five to a line on FLRDAT using FORMAT(1X,5F10.3). For example, suppose the first flare is to be launched 2 seconds into the simulation, the next 1 second later, the third 3 seconds after the second, the fourth and fifth 2 seconds after the third, the sixth 3.5 seconds later, and the seventh 4.0 seconds after that. Then, continuing the previous example, LTIMP = 6 and lines 7 and 8 are

```
2.000     1.000     3.000     2.000     0.000
3.5000    4.000
```

Notice that the fifth figure is 0.0. That is the time difference between ejection of the fourth and fifth flare. If KFLRT is more than 7, the eighth flare would be ejected 1 second after the seventh, the ninth 3 sec. later; i.e., the pattern established by the first seven would be repeated until the flare supply is exhausted. LANGP and LTIMP are not required to agree. The actual ejection times, measured from the start of the simulation are stored in DECTIM, i.e., DECTIM(K) is the time at which the Kth flare will be ejected.

The FLRDAT file is also used to input physical characteristics of the flares. These parameters are entered as functions of time by inputing tables of their

values at user specified times after ejection. The FLARE routine then uses the time elapsed since ejection and linear interpolation to determine current values. The flares are assumed to be physically identical.

Five sets of data are required. Each set corresponds to a single parameter and consists of an integer and two tables of data. One table is an increasing set of time values, in seconds, the second is a table of values of the parameter at those time values. The integer is the number of elements in the time (or parameter) table. Each of the five sets of data are input in the same way. The integer is listed first using FORMAT(1X,I2). Next the table of time values is listed using FORMAT(1X,5E13.5), then the parameter values again using FORMAT(1X,5E13.5). The first of these sets on the input file TAPE9 = FLRDAT follows the ejection times already discussed. It is for a weight history, in pounds, of the flare. The time table is stored in FLTIM, the weight in FLWT. The initial weight table entry then would be the weight of the flare when ejected. The second set of data, stored in FLMACT and DRGCOE, is for the drag coefficient of the flare; the third, stored in TIMEAR and RFAREA, for aerodynamic cross section area in ft^2; the fourth, stored in TIMTHR and THRUST, is thrust in pounds; and the fifth, stored in TIMFLX and FLFLX, is related to in band energy produced by the flare. If DISAMS-1 is run in a mode that includes the attenuation of source signals due to distance, IRATN = 1 or 2, this parameter table should be the radiant intensity of the flare in watts/sr.; if attenuation due to distance is not used in DISAMS-1, IRATN = 0, the table should be the irradiance at the dome of the missile in watts/cm^2.

The last entry on the FLRDAT file is the ejection speed of the flares in ft/sec relative to the launching platform using FORMAT(1X,E13.5). An example of a FLRDAT file is shown in Figure 5.1-1.

The interpolation scheme used in the flare program expects the time variable to lie in the range of the time table for each parameter. It is, then, good practice to set the last time value (lines 10, 13, 16, 19 and 22 in Figure 5.1-1.) equal to at least the maximum simulation time. The default value for that time is 20.0 seconds in DISAMS-1.

5.2 Subroutine Communication and Calculation

Communication between the subroutines making up the flare model and the subroutines of DISAMS-1 is accomplished primarily through common blocks. Input of initial parameters was described in the previous section. The current values of a number of other variables defined in DISAMS-1 are also required. Tables 5.2-1 and 5.2-2 display the variables referenced or defined in subroutines FDECOY and FLARE respectively which are also referenced or defined in other subroutines. NFLR is the parameter used by DISAMS-1 to determine whether or not the flare model is to be exercised. If NFLR $\neq$ 0, the model is called, if NFLR = 0, it is not.

The flare model is initialized by a call to entry IFDEC in FDECOY. In addition to assigning values to several other variables, values of KFLRT, LANGP, LTIMP, EALPHA, EBETA, FLX0, FLY0, FLZ0, and DECTIM are read from the TAPE9 = FLRDAT file and extended by periodicity as described earlier. A call to entry IFLAR in FLARE is

then made to initialize that subroutine. This call results in data on the FLRDAT file being assigned to the five sets of parameters associated with flare weight, drag coefficient, effective area, thrust, and infrared energy. The flare ejection speed, EV, is also read. The flare weight is expressed in pounds, effective area in square feet, thrust in pounds, and the inband energy in watts/steradian if atmospheric and range attenuation are included in the simulation, in watts/cm^2 if atmosphere and range are ignored. Time is in seconds and speed in ft/sec.

A call to FDECOY is made on each call of SEEKER and results in a comparison of T, the current simulation time, to entries in DECTIM, the flare launch times, to determine if a flare is to be ejected. If so, KE, the index of the highest numbered active flare, is incremented by one for each flare added to the active list. For each of these new flares, a call to FLARE is made to initialize the variables associated with its launch. A record of the ejection time T is stored in T0(NFL) where NFL is the index of the flare. The earth coordinates of the flare are determined by the earth coordinates of the launching platform (TX, TY, TZ) and the coordinates (FLX0, FLY0, FLZ0) of the flare relative to the launching platform. Velocity is derived from the velocity of the platform (DTX, DTY, DTZ), the ejection speed, EV, and the azimuth and elevation of the flare velocity relative to the launching platform, EBETA and EALPHA, as well as the orientation of the launching platform itself. If it is determined that all flares have been expended and are out of twice the FOV of the seeker, NFLR is set equal to zero and no additional calls to

FDECOY are made.

FDECOY then makes a call to FLRPOS in the FLARE subroutine for each active flare. This results in the calculation of values for arrays XFP, YFP, and ZFP the earth coordinates of the flares. In addition to these variables, flare acceleration, velocity, and intensity are updated. The azimuth and elevation of the flare trajectory are also available. These variable values are calculated using standard aerodynamic relations and equations of motion. The parameter values of weight, drag coefficient, effective area, and thrust are calculated using the linear interpolation routine TLU, the current value T of simulated time, and the time of launch of each flare T0(NFL).

After the return to FDECOY and beginning with the active flare of lowest index, KB, a call to RETCOR is made. This call returns the rectangular coordinates XDEC, YDEC and the polar coordinates RDEC and THDEC of the image of that flare on the reticle plane. If the flare is outside twice the FOV of the seeker, that flare is dropped from the active list and is no longer tracked. The process is repeated for all flares up to index KE, if there are any. At the conclusion of this loop then, KB is set equal to the index of the lowest indexed active flare and KE is the index of the highest indexed active flare. If no such flares exist, i.e., if the active flare list is empty, a RETURN is made.

For each of the active flares, a check is next made to determine whether or not it is in the FOV. If the index of the flare is NFL and the flare is in the FOV, INFOV(NFL) is set equal to 1, if not in the FOV, INFOV(NFL) = 0. Note that all active flares are tracked,

but some or even all of these flares may be outside the FOV and thus have no effect on seeker signals. Whenever a flare either enters or leaves the field of view, an informative message is written on the OUTPUT file stating the flare index and the simulation time when the event occurred.

The flare signal strength, DECFLX, which was calculated in FLARE for each flare in the FOV is now modified by multiplying by ATENU, which is the atmospheric attenuation, and by dividing by the square of the distance from the missile to the flare. If IRATN is zero, this step is omitted. A call to RSIG determines the portion of the flare signal strength that is transmitted through the reticle, and DECSIG, the detector signal due to the flare, is then calculated by multiplying the modified value of DECFLX by the reticle transmission factor. A RETURN is then made to the calling program.

5.3 Output

Neither FDECOY nor FLARE output data for printing directly except for the messages indicating when flares enter and leave the FOV. As implemented in DISAMS-1 however, if the parameter NPATH = 1, data from these routines are written on the file TAPE19 = TXYZ every 0.1 sec. of simulated time. At each time interval, a line containing values of

T, KTOT, AMXE, AMYE, AMZE, TX, TY, TZ

using FORMAT(1X,F7.3,I3,3X,6(1X,F9.1)) is printed. T is the simulated time in seconds, KTOT is the number of

flares within twice the FOV; AMXE, AMYE, AMZE are the earth coordinates of the missile; and TX, TY, TZ are the earth coordinates of the launch platform or target. The next line contains

PHMB, THMB, PSMB, PHT, GMT, PST

using FORMAT(14X,6(1X,F9.1)) where PHMB, THMB and PSMB are roll, pitch, and yaw of the missile in degrees and PHT, GMT, and PST are roll, pitch, and yaw of the target, also in degrees.

If KTOT is positive, the next KTOT lines have the form

I, INFOV(I), XFP(I), YFP (I), ZFP(I), DECFLX(I)

using FORMAT(8X,2I3,3(1X,F9.1),1X,E12.5). The integer I indicates the index of the flare represented by the data of that line. If INFOV(I) = 0, the flare is outside the FOV, but within twice the FOV. If INFOV(I) = 1, the flare is in the FOV and contributes to seeker signals. XFP(I), YFP(I), and ZFP(I) are the earth coordinates of the flare and DECFLX(I) is either the flare radiant intensity or its irradiance at the missile dome, depending on how the flux array FLFLX was defined on the FLRDAT file.

The next line printed begins a repetition of the pattern just described. Note that if KTOT = 0, only two lines are printed for each time value. If the flare model is not used, KTOT = 0 by default. An example of output from this file is shown in Figure 5.3-1.

```
42  5  6
  -90.000      0.000    -10.000      0.000      5.000
    0.000     90.000      0.000      5.000      3.000
    0.000     90.000      0.000      5.000      3.000
    0.000    -90.000      0.000     -5.000      3.000
  -45.000    -90.000      0.000     -5.000      3.000
    2.000      1.000      3.000      2.000      0.000
    3.500      4.000
3
 0.              .20000E+01    .20000E+02
  .85000E+01     .50000E+01    .50000E+01
2
 0.              .20000E+02
  .60000E+00     .60000E+00
2
 0.              .20000E+02
  .72000E-01     .72000E-01
2
 0.              .20000E+02
 0.             0.
2
 0.              .20000E+02
  .10000E-07     .10000E-07
  .76000E+02
```

Figure 5.1-1 Example of a FLRDAT input file.

Variable	Common Block	Defined or Referenced	Definition
AHXP	ATMX	D	Average altitude of missile and flare. Used in ATMSX.
AMXE AMYE AMZE	YDY	R	Missile earth coordinates.
ARXP	ATMX	D,R	Distance from missile to flare. Used in ATMSX.
ATRNG	FLXCOM	R	Minimum change in distance between flare and missile for ATMSX call to be made. Defined in CHANGE.
ATX	ATMX	R	An array containing the atmospheric transmission coefficient. Defined in ATMSX. ATX(2) is the element used in FDECOY.
DANG	DECOM	R	Array of angles representing angular positions of the reticle at which transmission is calculated. Defined in SEEKER.
DECFLX	SUBVAR	R	Array of either radiant intensity or irradiance values due to a flare. Defined in FLARE. If DECFLX represents radiant intensity, IRATN should be 1 or 2, if DECFLX represents irradiance, IRATN should be Ø.
EALPHA	FLRVAR	D	Array of ejection elevation angles of the flares.
EBETA	FLRVAR	D	Array of ejection azimuth angles of the flares.
FLXØ FLYØ FLZØ	FLRVAR	D	Arrays of coordinates of flare ejection mechanisms in launch platform coordinates.

Table 5.2-1(a) Variables passed to or from FDECOY.

Variable	Common Block	Defined or Referenced	Definition
INFOV	DECOM	D,R	An array. if the Kth element is 1, the Kth flare is in the FOV of the missile; if Ø, the flare is outside the FOV.
ITH	DECOM	R	Integer defining current time interval.
JSIG	VARI	D	An integer identifying the flare for which RSIG is called.
KB	DECOM	D,R	The lowest numbered flare that is within twice the FOV of the missile.
KE	DECOM	D,R	The highest numbered flare that is within twice the FOV of the missile.
KTOT	DECOM	D,R	Defined by KE-KB+1, i.e. the number of active flares.
NDECAT	FLXCOM	R	If IRATN is nonzero, atmospheric and range attenuation is imposed on the flare signal DECFLX and NDECAT=1. If IRATN =Ø, it is assumed the flare signal is an irradiance at the dome of the missile and NDECAT=Ø. The value is set by the calling program.
NFL	SUBVAR	D	Integer identifying the flare being processed.
NFLR	DECOM	D	If NFLR=Ø. the flare subroutines are not called. NFLR is defined in CHANGE. To use the flare model, set NFLR=1. The default is Ø. When all flares are ejected and out of twice the FOV, NFLR is set equal to Ø.
NTIR	ATMX	D	An integer having the value of 2 in FDECOY and identifies the element of ATX used for atmospheric attenuation constant for flares.

Table 5.2-1(b) Variables passed to or from FDECOY (cont).

Variable	Common Block	Defined or Referenced	Definition
T	TVARYP	R	Current simulation time.

Table 5.2-1(c) Variables passed to or from FDECOY (cont).

Variable	Common Block	Defined or Referenced	Definition
DECFLX	SUBVAR	D,R	If IRATN=Ø, DECFLX represents irradiance of the missile dome by a flare. If IRATN is not zero, DECFLX is the radiant intensity of a flare.
DTX DTY DTZ	YDY	R	Target velocity in earth coordinates.
EALPHA	FLRVAR	R	An array of ejection elevation angles for the flares.
EBETA	FLRVAR	R	An array of ejection azimuth angles for the flares.
FLXØ FLYØ FLZØ	FLRVAR	R	Arrays of the coordinates in the launch platform coordinate system of flare ejection mechanism positions.
NFL	SUBVAR	R	An integer identifying the flare being processed.
QTB	ANGMAT	R	A 3x3 coordinate transformation matrix from launch platform coordinates to earth coordinates.
T	TVARYP	R	Current simulation time.
TX TY TZ	YDY	R	Target coordinates in the earth coordinate system.
XFP YFP ZFP	SUBVAR	D,R	Arrays for the coordinates of the flares in the earth coordinate system.

Table 5.2-2 Variables passed to or from FLARE.

```
1.900  0        -3219.3    3489.4    -307.8     665.0      0.0    -3000.0
                  -87.2      16.0     -34.2       0.0      0.0        0.0
2.000  0        -3123.8    3429.5    -341.6     700.0      0.0    -3000.0
                 -144.6      16.3     -33.6       0.0      0.0        0.0
2.100  1        -3023.5    3365.9    -377.4     735.0      0.0    -3000.0
                  146.5      20.7     -35.2       0.0      0.0        0.0
       1  1       724.7       0.0   -2987.4   .10000E-07
2.200  1        -2919.8    3298.9    -415.3     770.0      0.0    -3000.0
                   85.3      15.3     -35.3       0.0      0.0        0.0
       1  1       759.3       0.0   -2979.4   .10000E-07
2.300  1        -2813.7    3229.0    -453.9     805.0      0.0    -3000.0
                   30.9      22.3     -36.9       0.0      0.0        0.0
       1  1       793.6       0.0   -2971.1   .10000E-07
2.400  1        -2706.8    3157.4    -494.2     840.0      0.0    -3000.0
                  -15.6      17.7     -36.2       0.0      0.0        0.0
       1  1       827.7       0.0   -2962.6   .10000E-07
2.500  1        -2599.5    3084.6    -535.1     875.0      0.0    -3000.0
                  -54.9      16.0     -35.4       0.0      0.0        0.0
       1  1       861.5       0.0   -2953.9   .10000E-07
2.600  1        -2492.0    3010.9    -576.0     910.0      0.0    -3000.0
                  -82.1      22.3     -31.4       0.0      0.0        0.0
       1  1       895.0       0.0   -2944.9   .10000E-07
2.700  1        -2384.2    2937.4    -618.0     945.0      0.0    -3000.0
                  -97.4      19.0     -33.9       0.0      0.0        0.0
       1  1       928.2       0.0   -2935.6   .10000E-07
2.800  1        -2276.0    2863.5    -660.4     980.0      0.0    -3000.0
                  -96.9      17.4     -32.4       0.0      0.0        0.0
       1  1       961.2       0.0   -2926.1   .10000E-07
2.900  1        -2167.2    2789.2    -702.6    1015.0      0.0    -3000.0
                  -82.5      19.7     -32.8       0.0      0.0        0.0
       1  1       993.9       0.0   -2916.4   .10000E-07
3.000  1        -2058.0    2714.8    -745.2    1050.0      0.0    -3000.0
                  -54.1      17.2     -34.1       0.0      0.0        0.0
       1  1      1026.3       0.0   -2906.4   .10000E-07
3.100  2        -1948.5    2639.8    -788.0    1085.0      0.0    -3000.0
                  -10.2      24.2     -32.9       0.0      0.0        0.0
       1  1      1058.4       0.0   -2896.2   .10000E-07
       2  1      1084.7      12.5   -2996.8   .10000E-07
3.200  2        -1838.7    2565.0    -831.7    1120.0      0.0    -3000.0
                   47.2      14.8     -34.0       0.0      0.0        0.0
       1  1      1090.2       0.0   -2885.8   .10000E-07
       2  0      1119.3      20.0   -2996.4   .10000E-07
3.300  2        -1728.3    2489.6    -874.3    1155.0      0.0    -3000.0
                  119.0      16.8     -35.7       0.0      0.0        0.0
       1  1      1121.7       0.0   -2875.1   .10000E-07
       2  0      1153.6      27.4   -2995.6   .10000E-07
3.400  1        -1617.7    2413.6    -916.8    1190.0      0.0    -3000.0
                 -153.0      20.6     -31.2       0.0      0.0        0.0
       1  1      1152.9       0.0   -2864.2   .10000E-07
3.500  1        -1506.4    2338.4    -960.2    1225.0      0.0    -3000.0
                  -53.0      18.5     -33.5       0.0      0.0        0.0
       1  1      1183.9       0.0   -2853.2   .10000E-07
```

Figure 5.3-1 A portion of a TXYZ output file.

6.0 Model Validation

Earlier reports have presented data that compares output produced by the seeker model to measurements and signal traces generated by actual hardware. Those data demonstrate that, at least under the conditions given, the model output and measured output are very similar. No comparisons have been reported, however, between missile trajectories generated by the model and measured trajectories. That this is a serious omission is well recognized.

Unfortunately, only limited data is available that is suitable for such a purpose. Due to the difficulty and expense of acquiring good telemetry data from a live firing, it is understandable that most of the firings are devoted to testing the missile against some kind of jammer or decoy. For the purpose of validation of the model, flights against flares are generally not useful, except in a limited way, since flare trajectories are not recorded. Tests involving active jammers are not useful either since the trajectory followed is strongly influenced by the relation between the reticle phase and that of the jammer. That data is not known.

There is, however, one set of firings that is useful for validation of the model. In the Spring of 1982 a number of refurbished missiles were fired to determine the effectiveness of a repair program and to obtain some information on the effects of long term storage. The tests were executed at the cable car

facility at Sandia. A total of eight missiles were fired against an infrared source mounted on the cable car. Due to a variety of equipment problems, only four of the tests are useful for model validation.

In each of these tests, a missile was fired at an IR source on the cable car. To protect the cable car, a flare was dropped in the terminal phase of the flight. Trajectory data was recorded for both the missile and the cable car. In one case, equipment failure resulted in early termination of trajectory recording. Table 6.0-1 records some of the pertinent information about these tests. A considerably more complete description can be found in the report of the test results (2).

DISAMS-1 is capable of using trajectories generated off-line for target position. To effect the simulations then, the cable car positions were inserted into the program as target positions as functions of time.

The coordinate system used to report the results is defined as follows. The origin is the launch point of the missile. The x axis is horizontal and perpendicular to the cable with the positive direction from the origin to the cable. The y axis is also horizontal and is parallel to the cable. The z axis is positive going away from the earth. The system is right handed.

Cable car positions for each of the tests are shown in Figure 6.0-1 and the velocities are shown in Figure 6.0-2. Note that for practical purposes, these trajectories are identical. Figures 6.0-3 to 6.0-6 compare the missile trajectories calculated by DISAMS-1 (the dotted lines) for each of the tests and the measured trajectories (the solid lines). Figure 6.0-7 displays all of this data on three graphs so that the overall results

can be seen. It is reassuring to note that the simulated trajectories fall within the envelope of the measured trajectories. Figures 6.0-8 to 6.0-12 display the velocity data.

These data do not provide absolute proof that the model will exactly imitate missile behavior in all situations nor is it claimed that it does so. In all of these firings, only moderate maneuvers were required of the missile to track the target. The data is reasonably convincing that in that case, the model imitates missile behavior fairly well. It is unfortunate that good data is not available for an encounter requiring more vigorous maneuvers.

Round	Super elevation (degrees)	Lead angle (degrees)	Background (cloud)	Flare ejection time after missile eject (seconds)
5	12.5	0	Cumulus	4.26
6	12.5	0	Blue/clear	4.30
7	12.5	0	Blue/clear	4.27
8	12.5	0	Blue/clear	4.86

Table 6.0-1 Parameters for live firings.

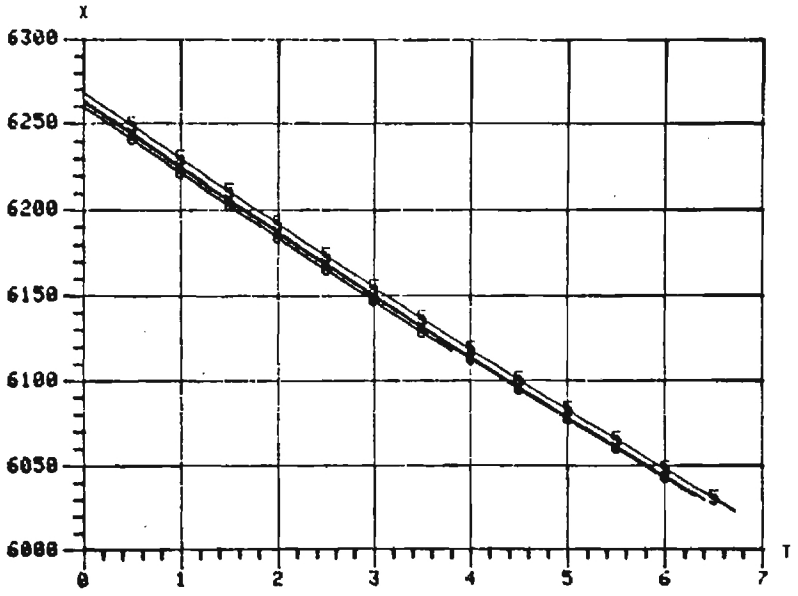

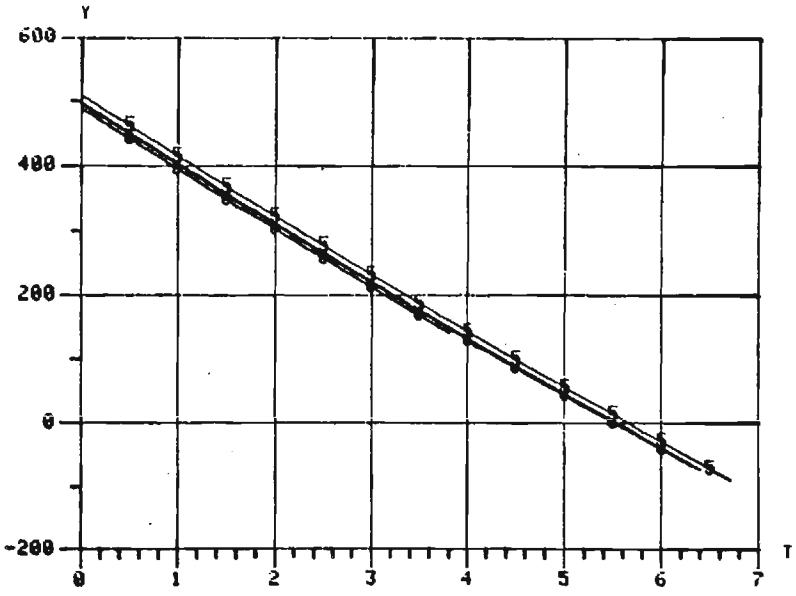

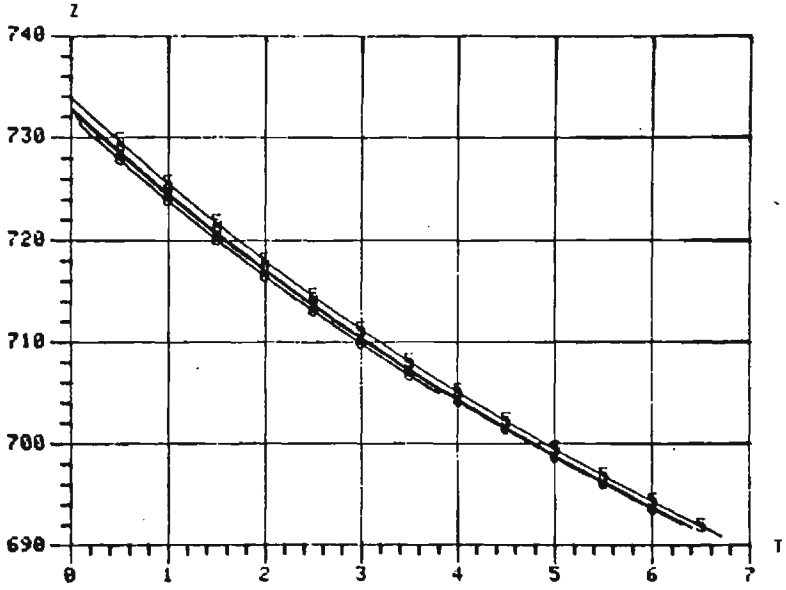

Vertical axis in feet
Horizontal axis in seconds

Figure 6.0-1 Cable car positions.

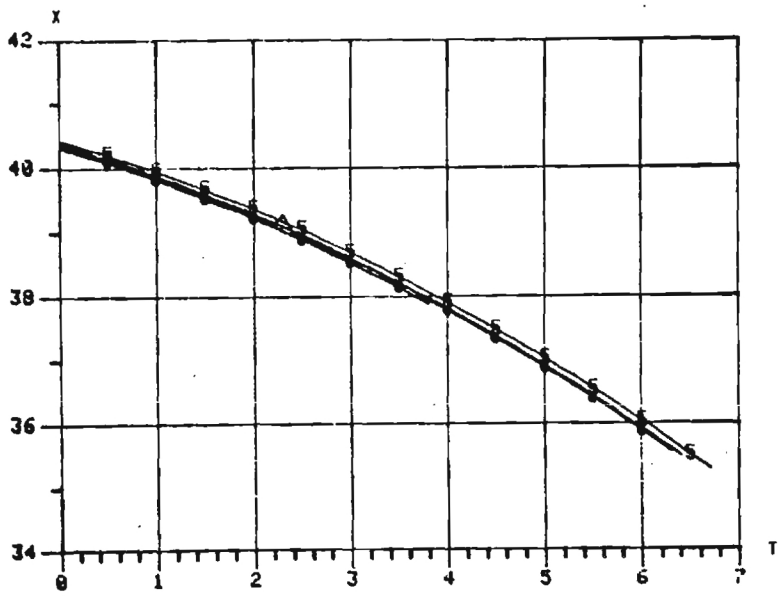

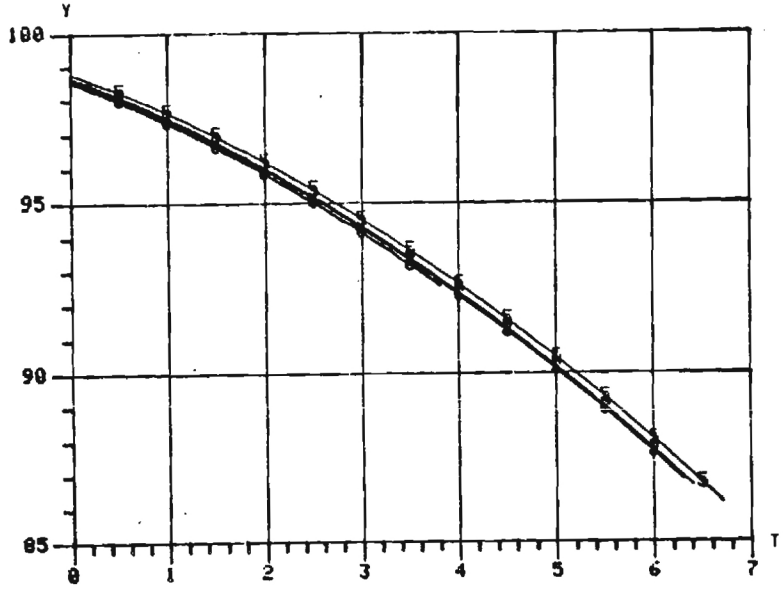

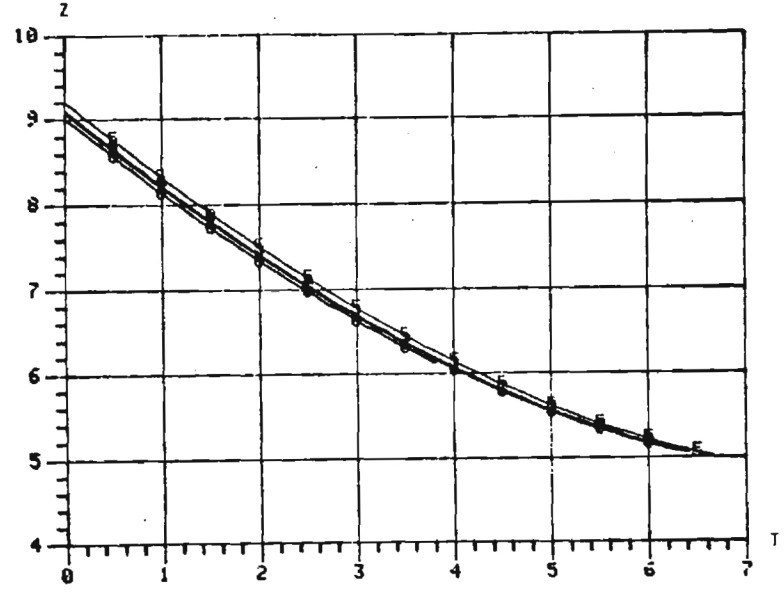

Vertical axis in feet/second
Horizontal axis in seconds

Figure 6.0-2 Cable car velocities.

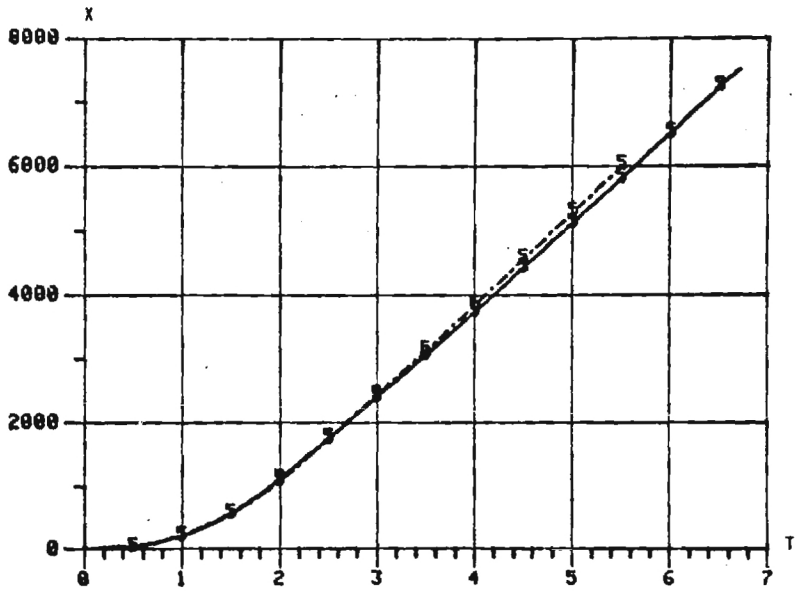

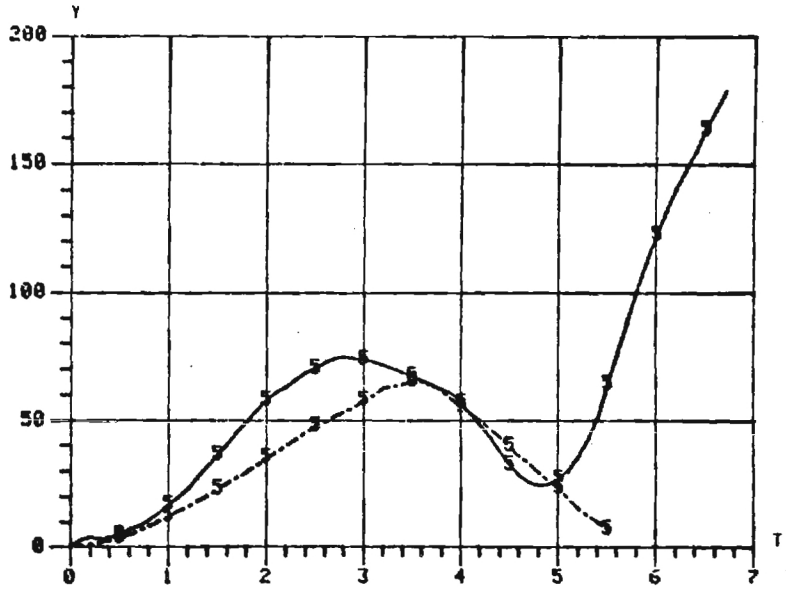

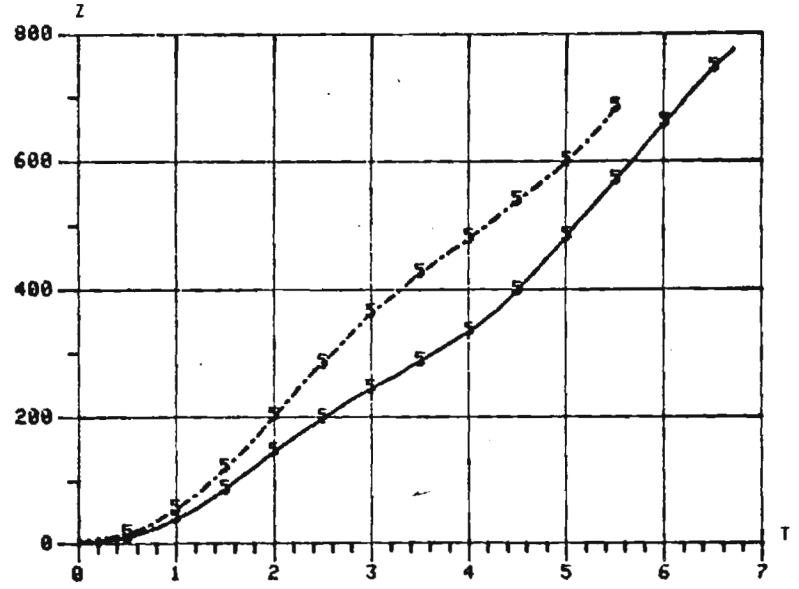

Vertical axis in feet
Horizontal axis in seconds
Solid line is telemetry data
Broken line is DISAMS-1 data

Figure 6.0-3 Measured and calculated positions for round #5.

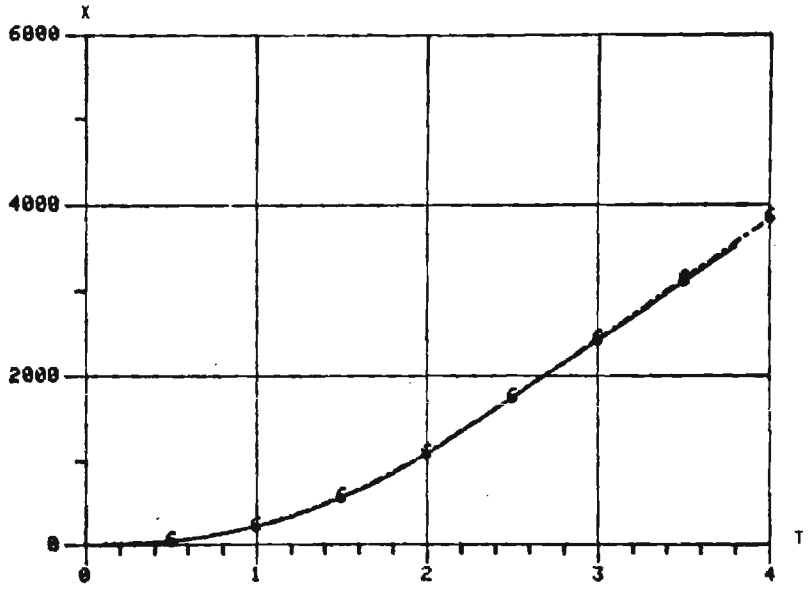

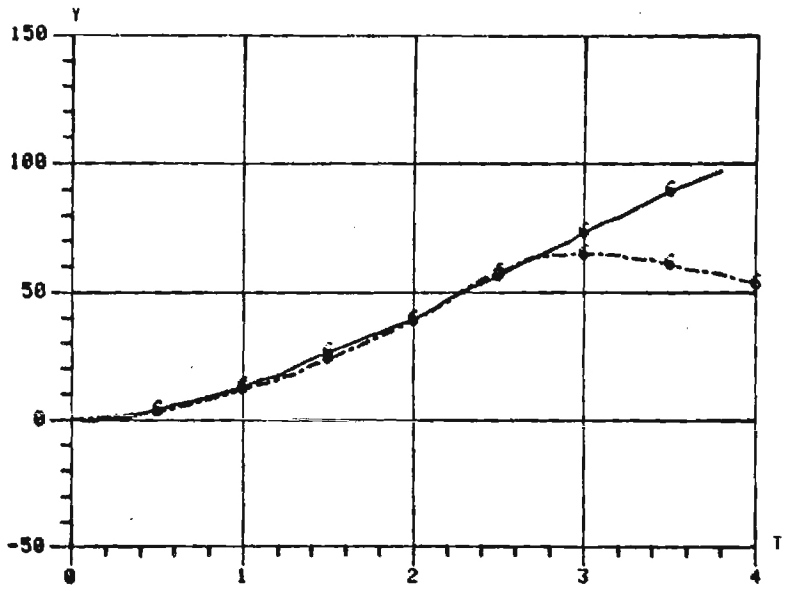

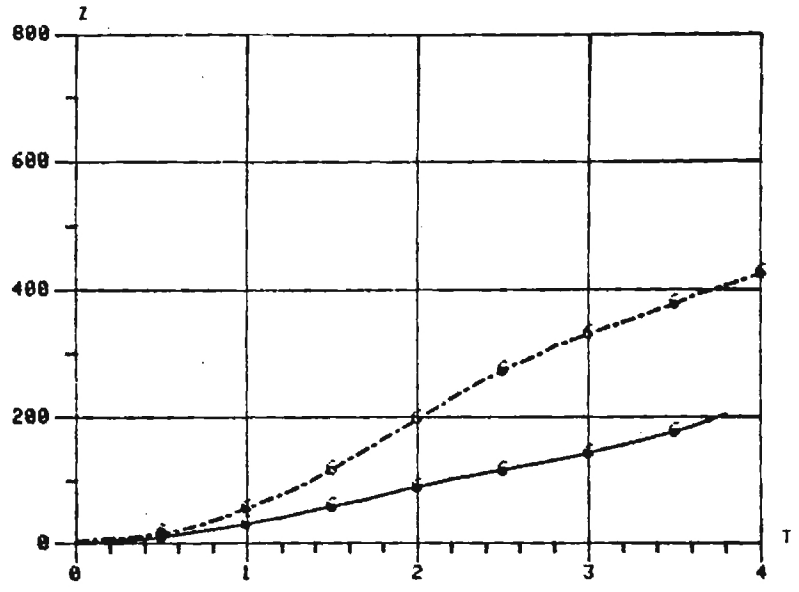

Vertical axis in feet
Horizontal axis in seconds
Solid line is telemetry data
Broken line is DISAMS-1 data

Figure 6.0-4 Measured and calculated positions for round #6.

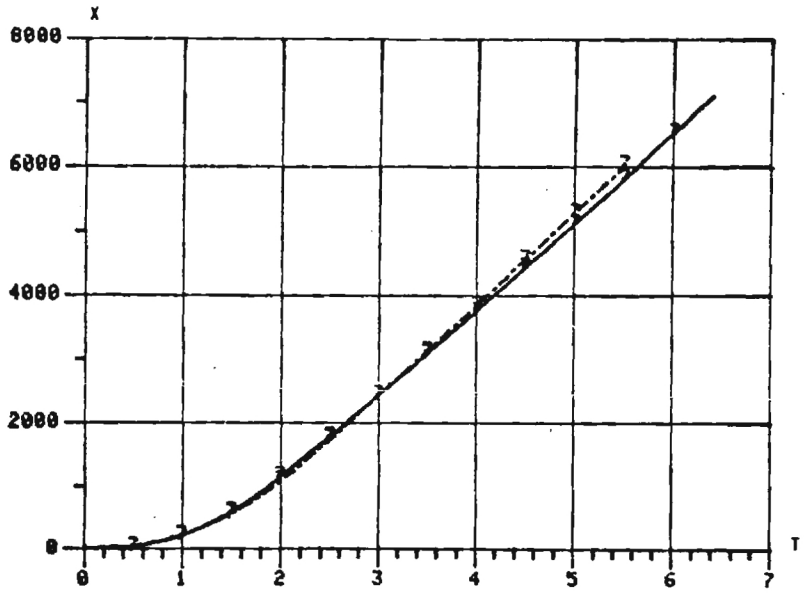

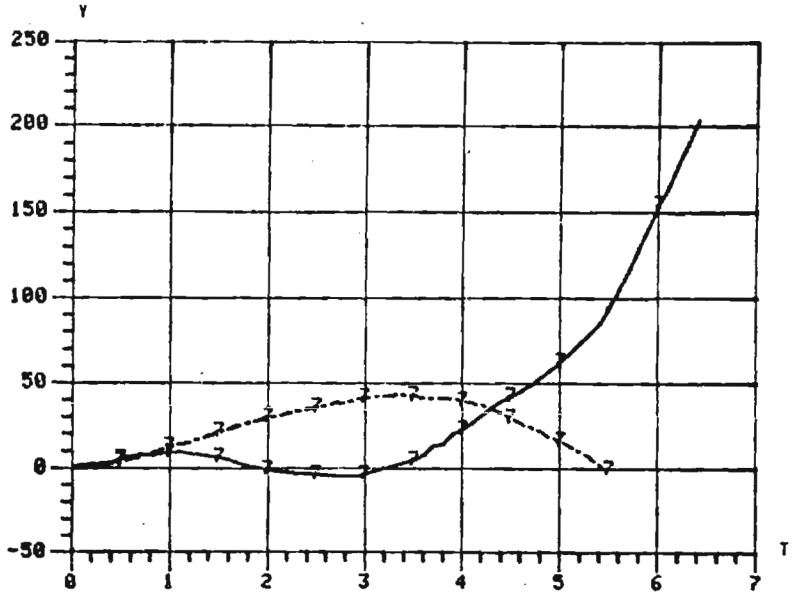

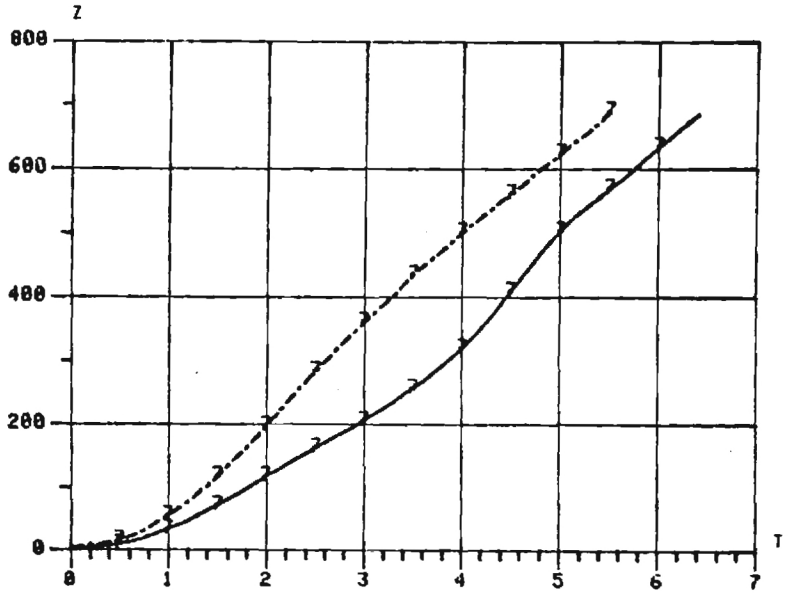

Vertical axis in feet
Horizontal axis in seconds
Solid line is telemetry data
Broken line is DISAMS-1 data

Figure 6.0-5 Measured and calculated positions for round #7.

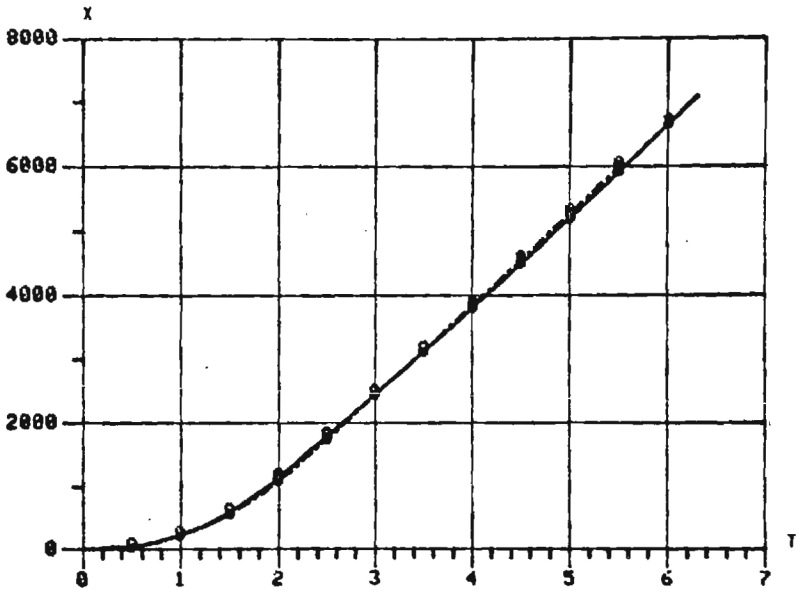

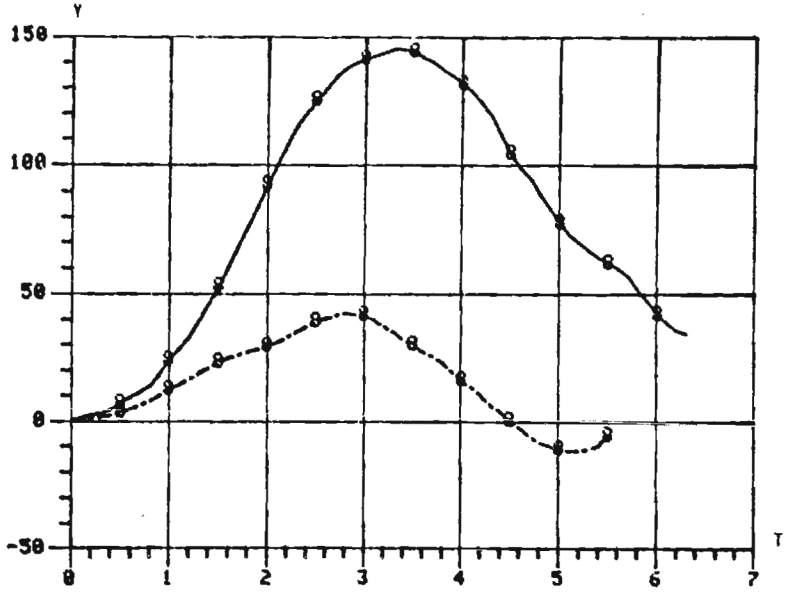

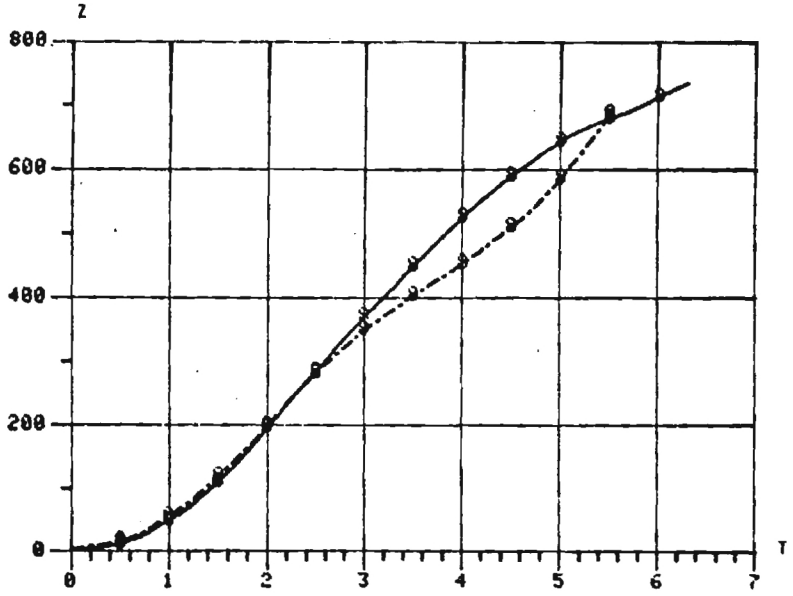

Vertical axis in feet
Horizontal axis in seconds
Solid line is telemetry data
Broken line is DISAMS-1 data

Figure 6.0-6 Measured and calculated positions for round #8.

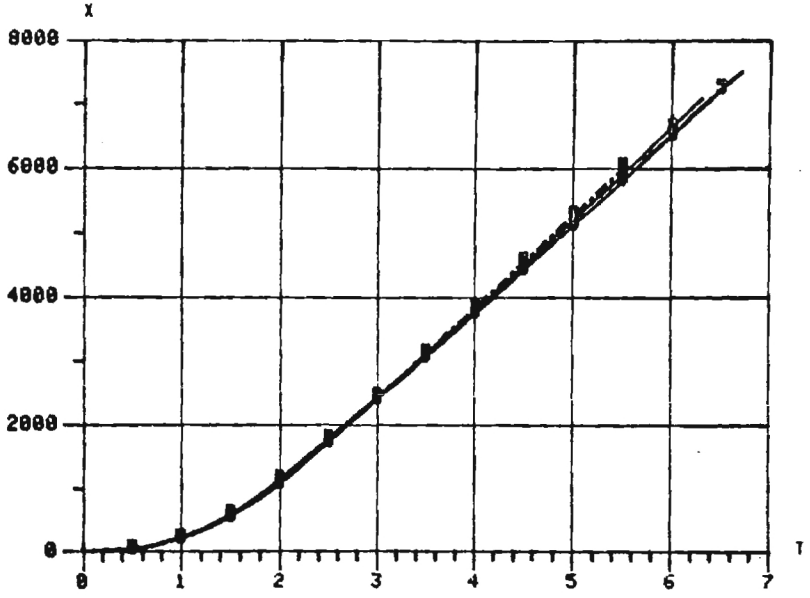

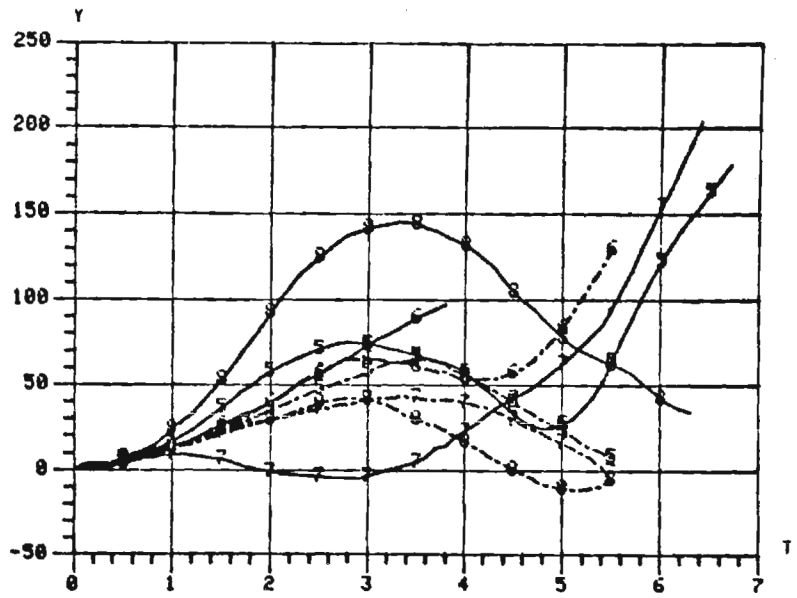

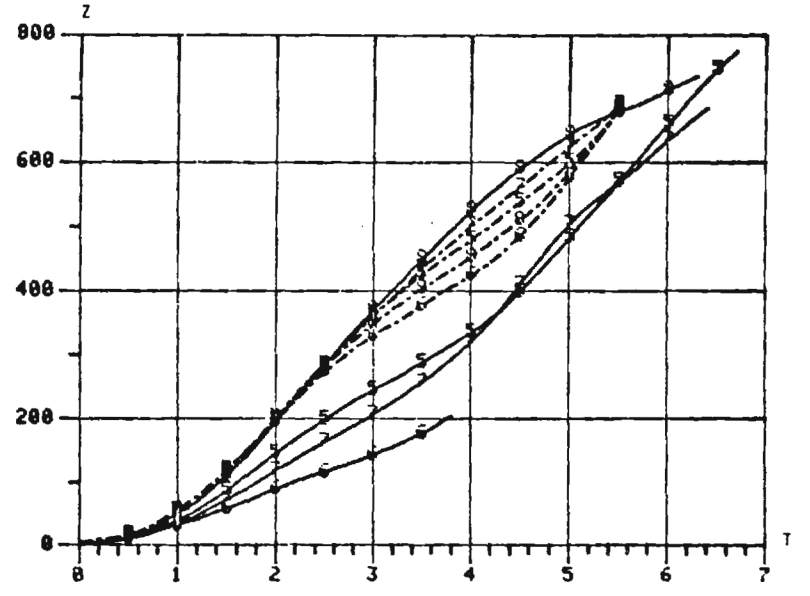

Vertical axis in feet
Horizontal axis in seconds
Solid line is telemetry data
Broken line is DISAMS-1 data

Figure 6.0-7 Measured and calculated positions summary.

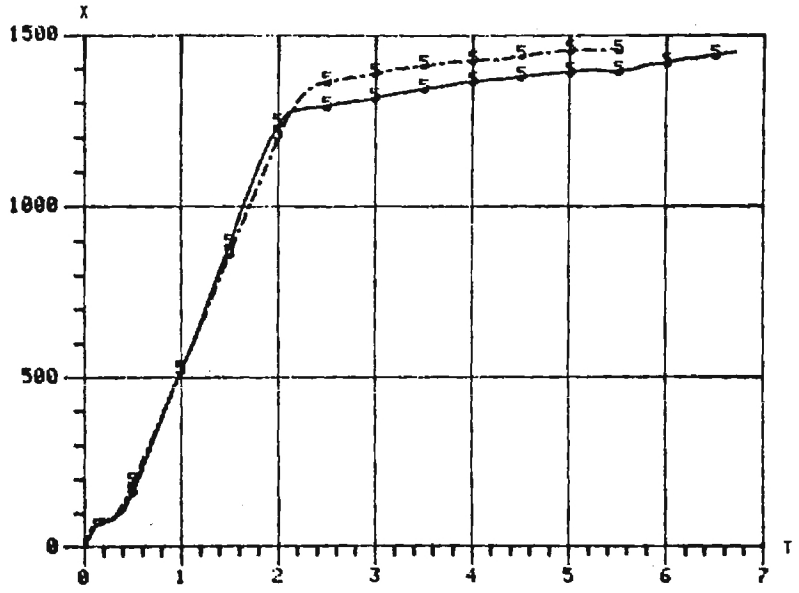

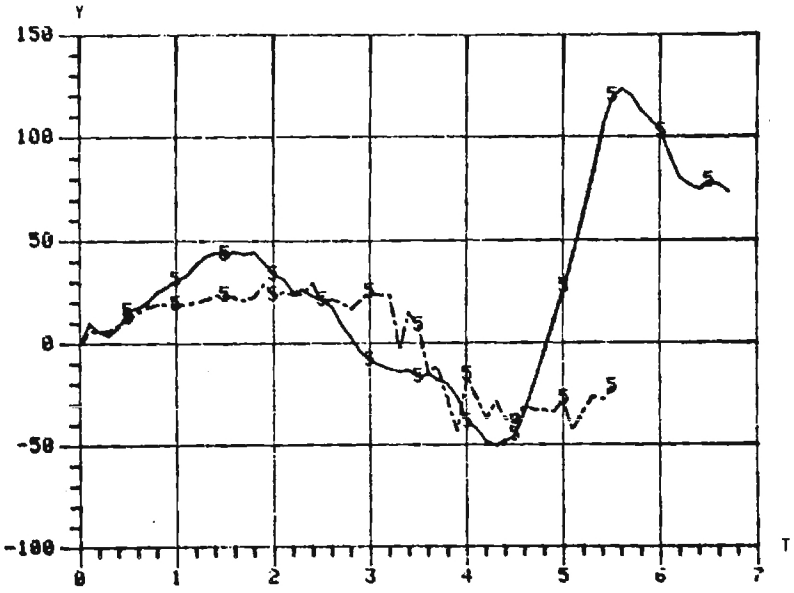

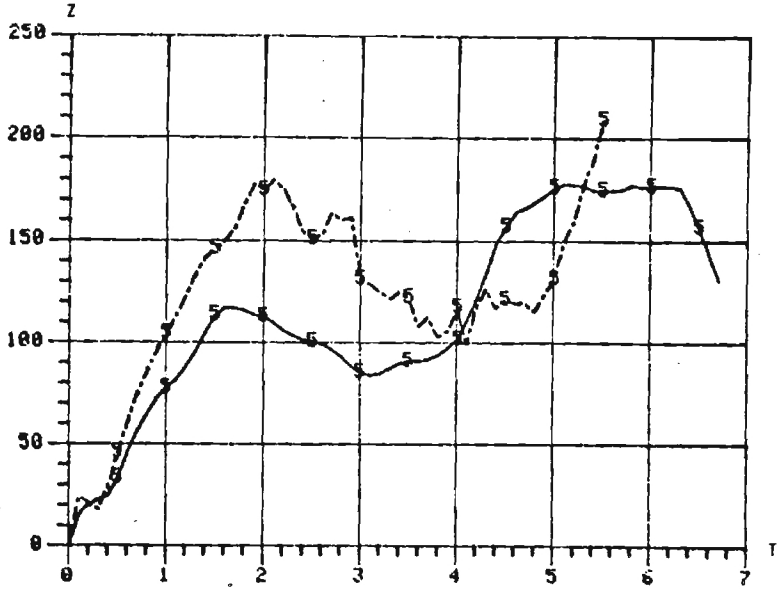

Vertical axis in feet/second
Horizontal axis in seconds
Solid line is telemetry data
Broken line is DISAMS-1 data

Figure 6.0-8 Measured and calculated velocities for round #5.

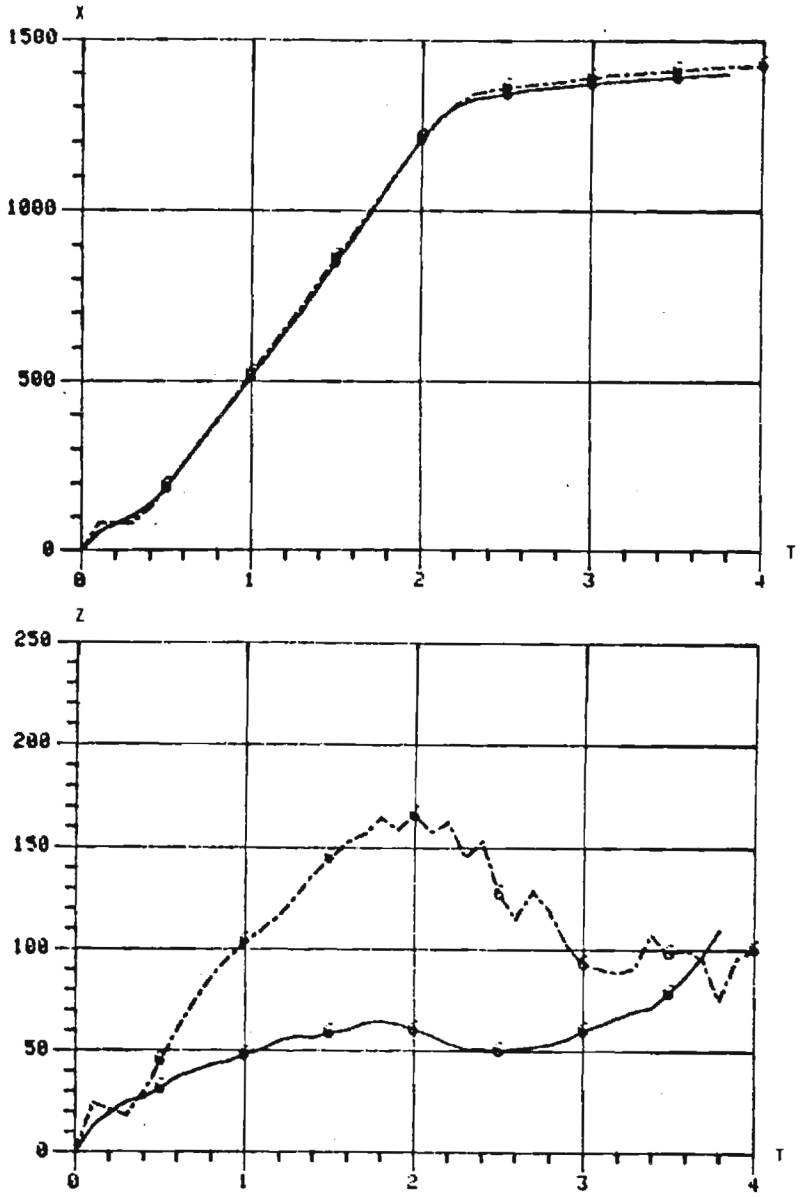

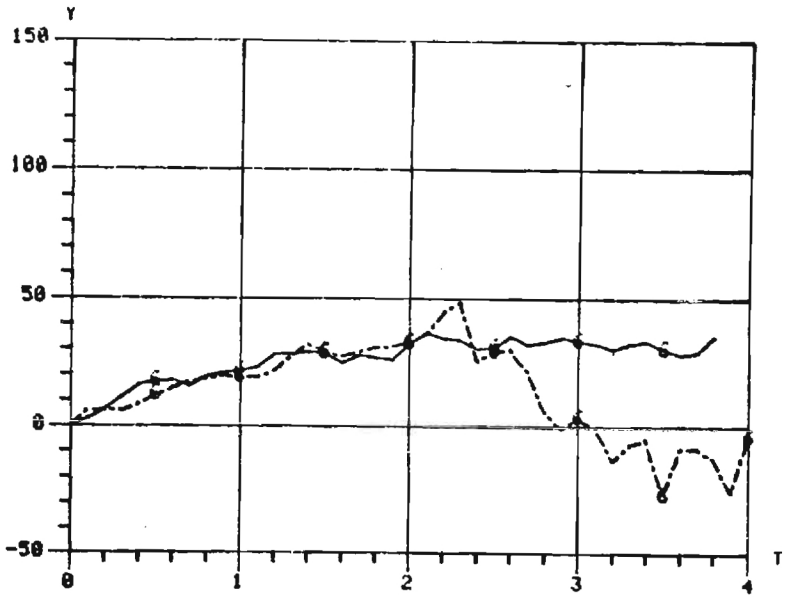

Vertical axis in feet/second
Horizontal axis in seconds
Solid line is telemetry data
Broken line is DISAMS-1 data

Figure 6.0-9 Measured and calculated velocities for round #6.

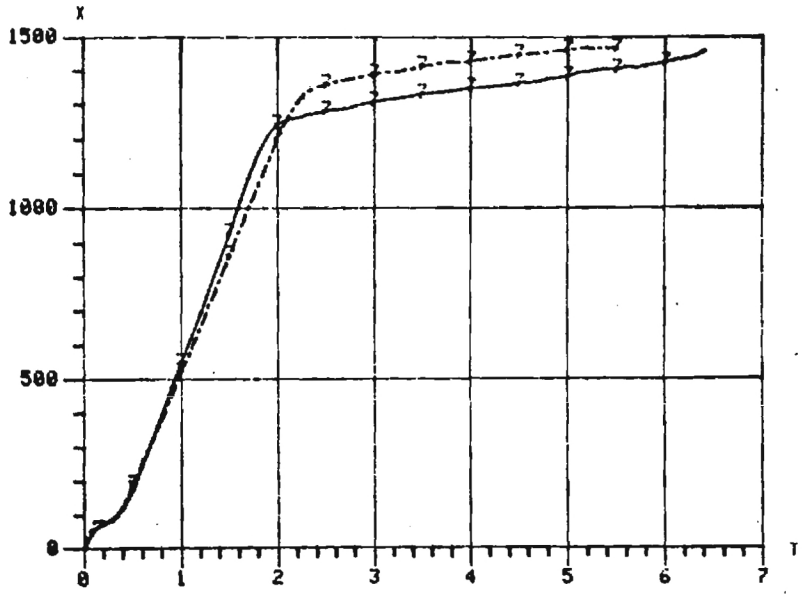

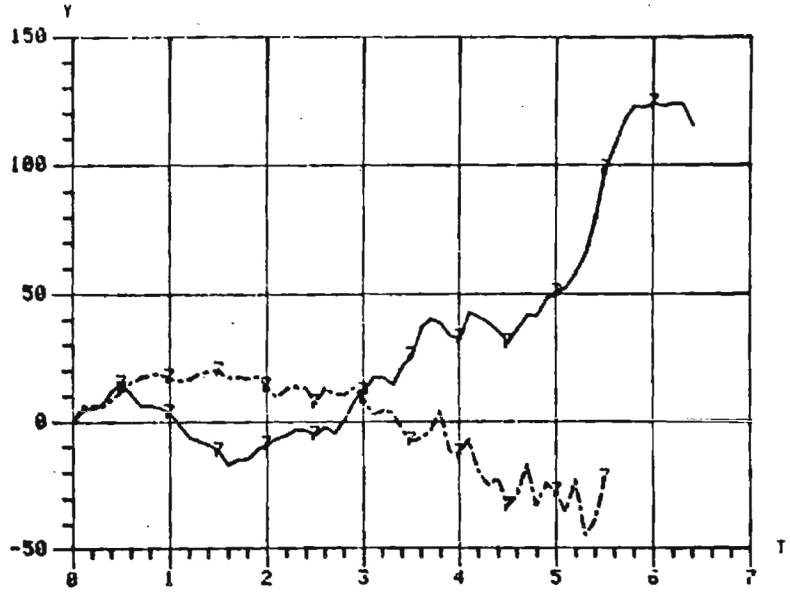

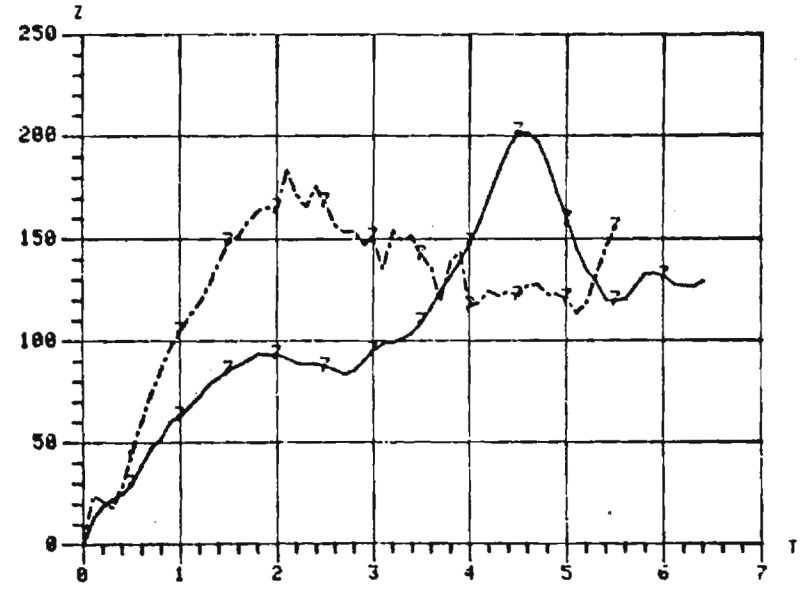

Vertical axis in feet/second
Horizontal axis in seconds
Solid line is telemetry data
Broken line is DISAMS-1 data

Figure 6.0-10 Measured and calculated velocities for round #7.

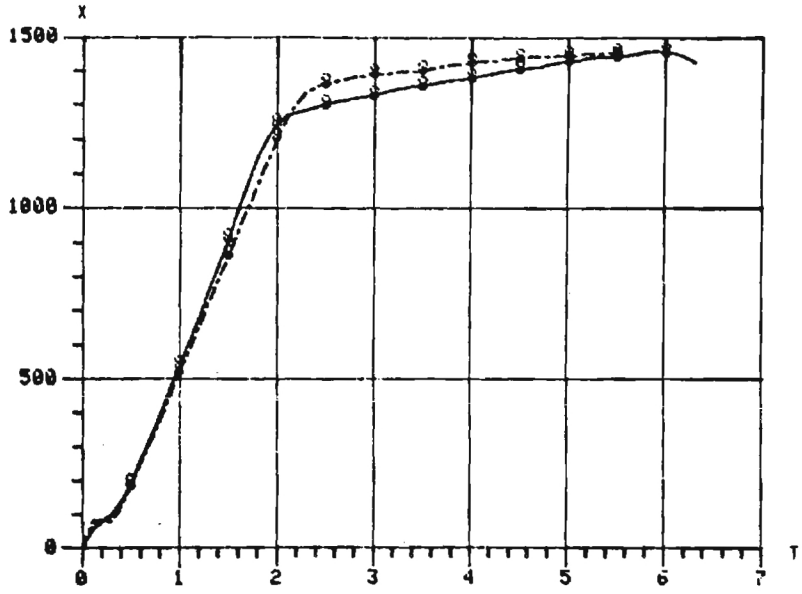

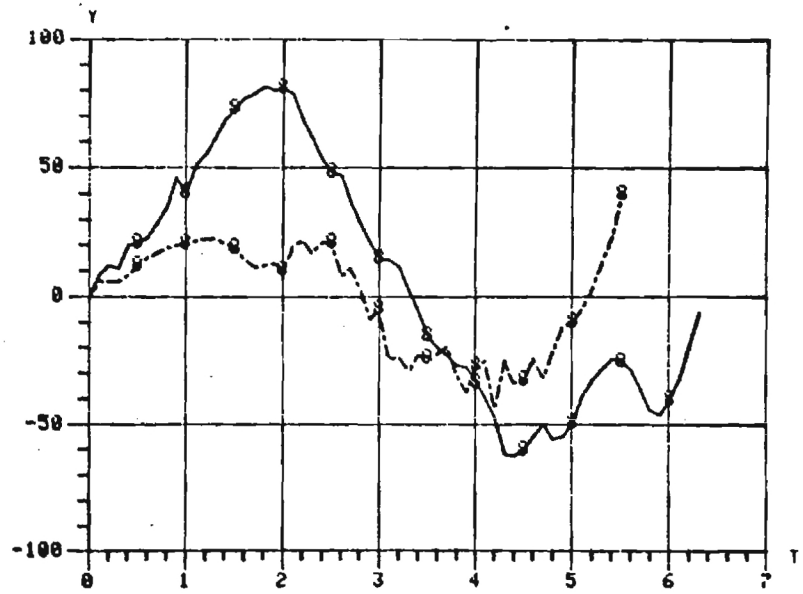

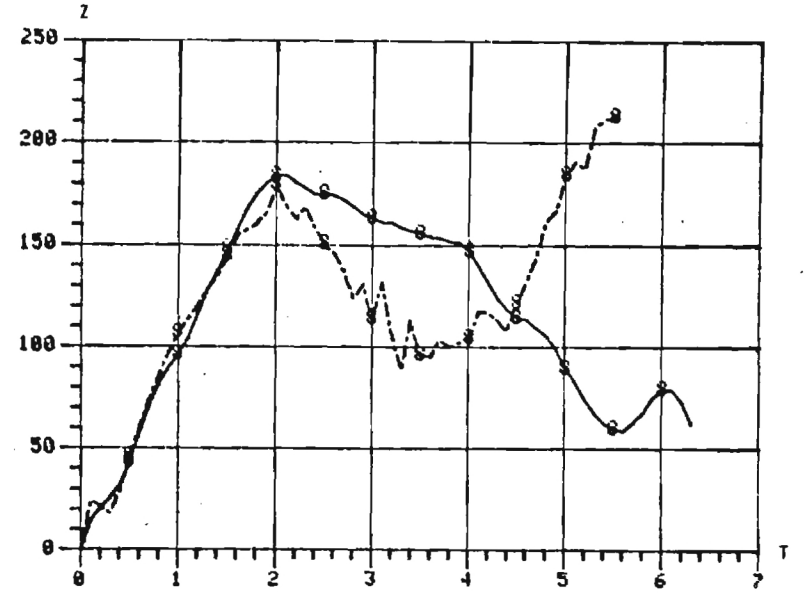

Vertical axis in feet/second
Horizontal axis in seconds
Solid line is telemetry data
Broken line is DISAMS-1 data

Figure 6.0-11 Measured and calculated velocities for round #8.

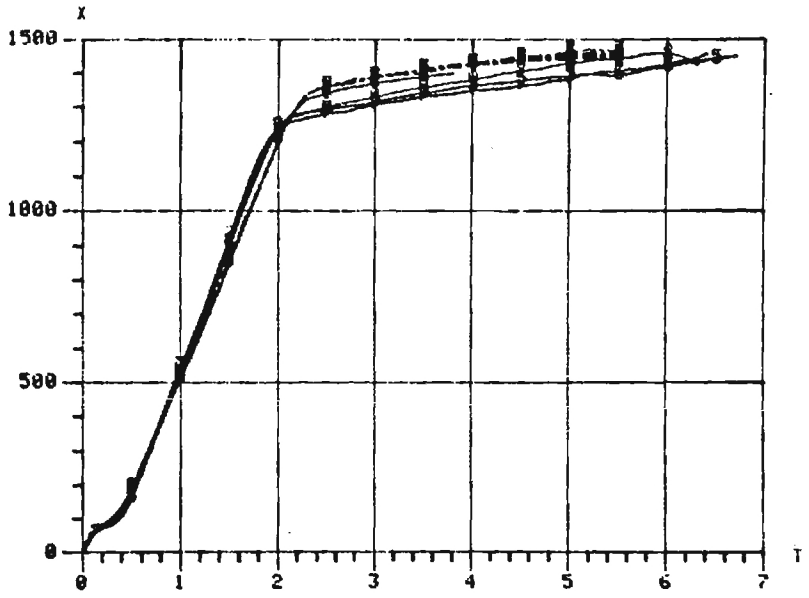

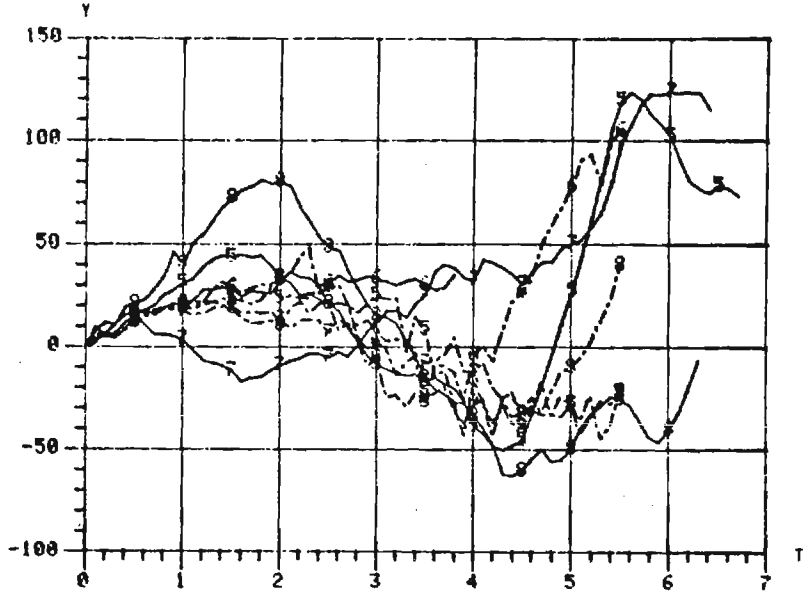

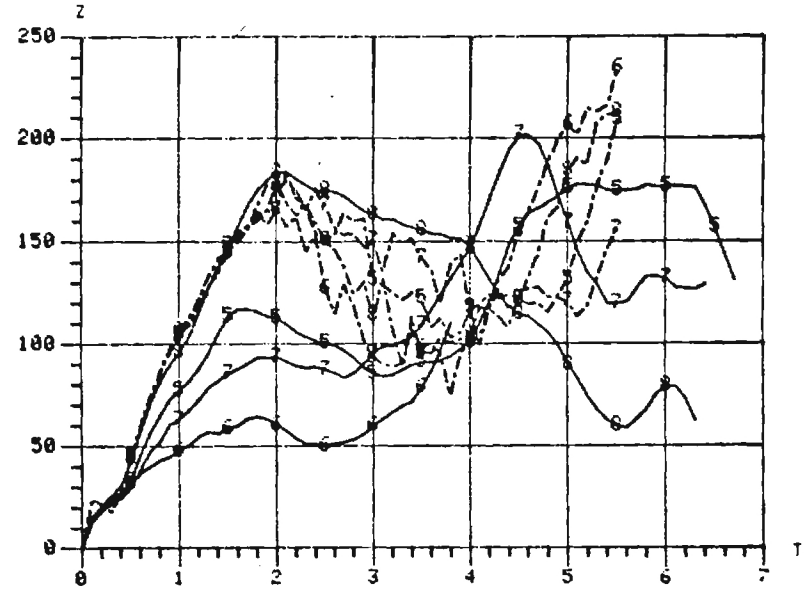

Vertical axis in feet/second
Horizontal axis in seconds
Solid line is telemetry data
Broken line is DISAMS-1 data

Figure 6.0-12 Measured and calculated velocity summary.

7.0 Footprint Predictions Using DISAMS-1

One of the uses for models like DISAMS-1 is to predict missile limits, maximum range, minimum launch distance, etc. DISAMS-1 has, in fact, been exercised in just this way to determine a "footprint" under specific conditions. These conditions in themselves were unrealistic, but the results obtained were subsequently merged with other data to compensate for the omissions. Only the DISAMS-1 predictions are presented here. The problem was to determine maximum and minimum launch ranges as functions of missile to target aspect angle for targets flying straight trajectories at various speeds and altitudes. The results were presented as a footprint of the missile successful launch area as seen from the target's perspective, i.e., the x,y axis origin was the target x,y position at the time of launch. If the missile is launched from a point within the inner and outer boundaries, a hit is predicted. For this series, a hit was taken to be a miss distance of six feet or less. Miss distance is the minimum distance obtained between the missile and the center of gravity of the target.

The function of DISAMS-1 in this case was to determine aerodynamic boundaries, so it was assumed that the target presented a strong IR signal to the missile regardless of aspect angle. As a consequence, a large forward aspect capability was predicted. The missile, in fact, does not have this capability but that is a conse-

quence of insufficient IR energy for the seeker to track rather than aerodynamic capacity.

Figures 7.0-1 to 7.0-12 show the results of the simulations. In most cases, the boundaries are surprisingly sharp in that between inner and outer boundaries, miss distances were quite small but increased rapidly as the missile launch position was moved outside those boundaries.

The matrix of Table 7.0-1 indicates the target altitude and speed for the individual figures. Where space is available on the figures, the miss distance is recorded for the simulation that had its launch position at that point. The last figure, Figure 7.0-13, shows all the footprints on a single page so that easy comparisons can be made.

Speed	100 ft	500 ft	5000 ft
500 kts	(1)	(2)	(3)
420 kts	(4)	(5)	(6)
390 kts	(7)	(8)	(9)
360 kts	(10)	(11)	(12)

Altitude

Table 7.0-1 Scenario identification for Figures 7.0-1 through 7.0-12.

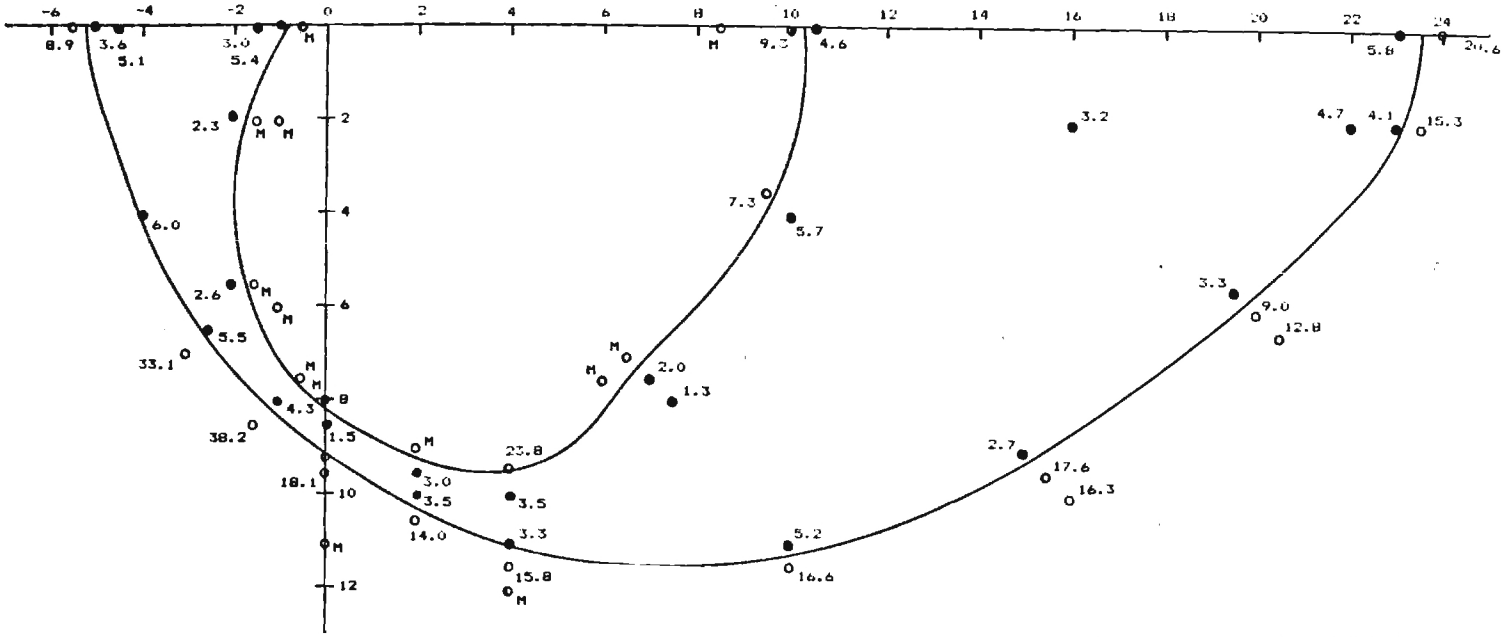

Target speed = 500 kts.
Target altitude = 100 ft.
Each division = 2000 ft.

Figure 7.0-1 Footprint for scenario #1.

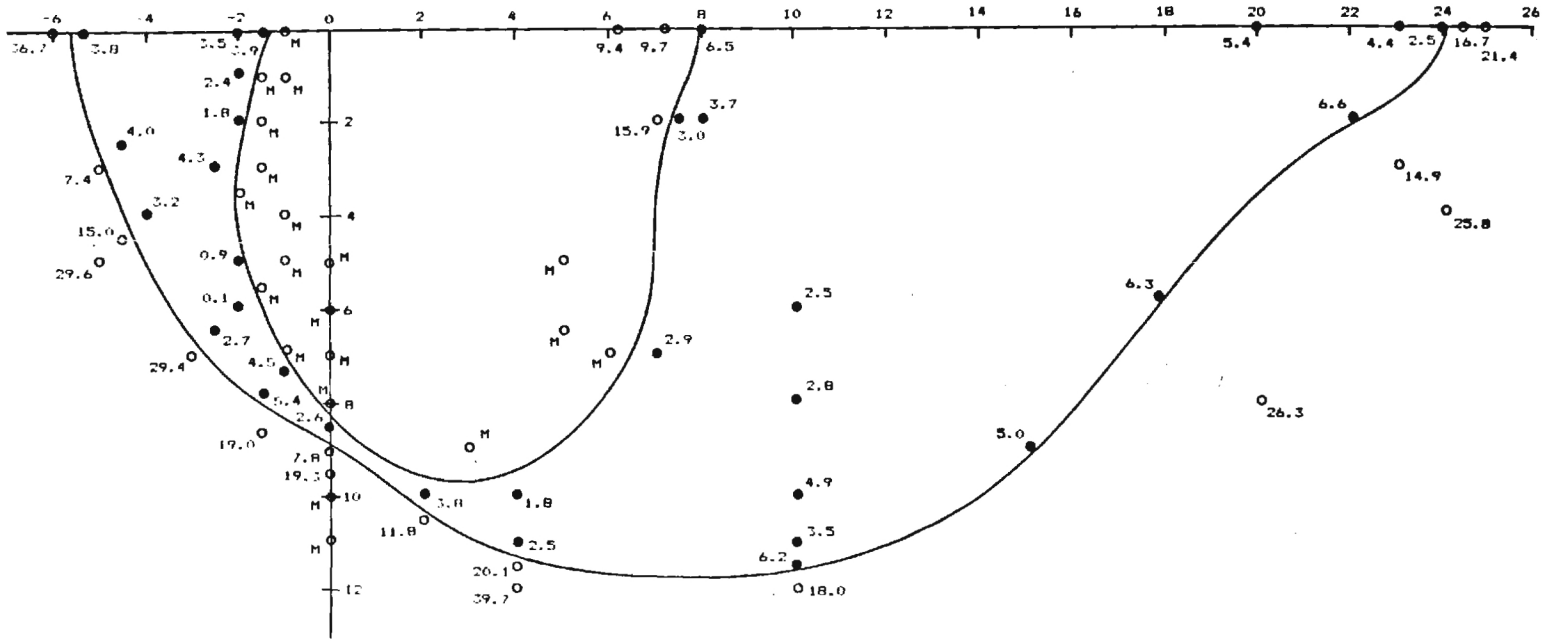

Target speed = 500 kts.
Target altitude = 500 ft.
Each division = 2000 ft.

Figure 7.0-2 Footprint for scenario #2.

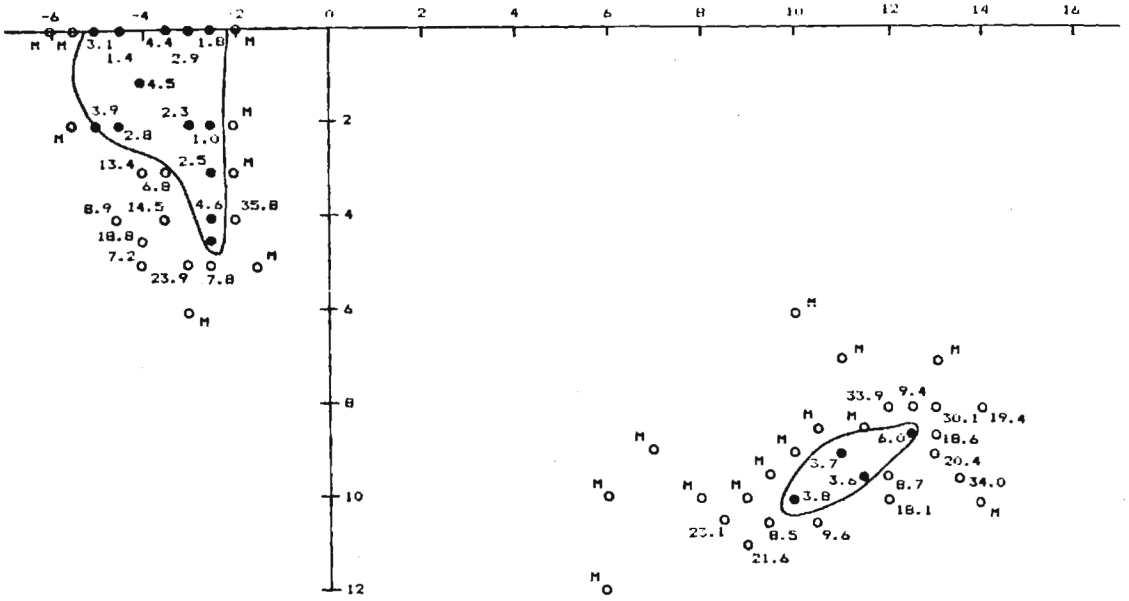

Target speed = 500 kts.

Target altitude = 5000 ft.

Each division = 2000 ft.

Figure 7.0-3 Footprint for scenario #3.

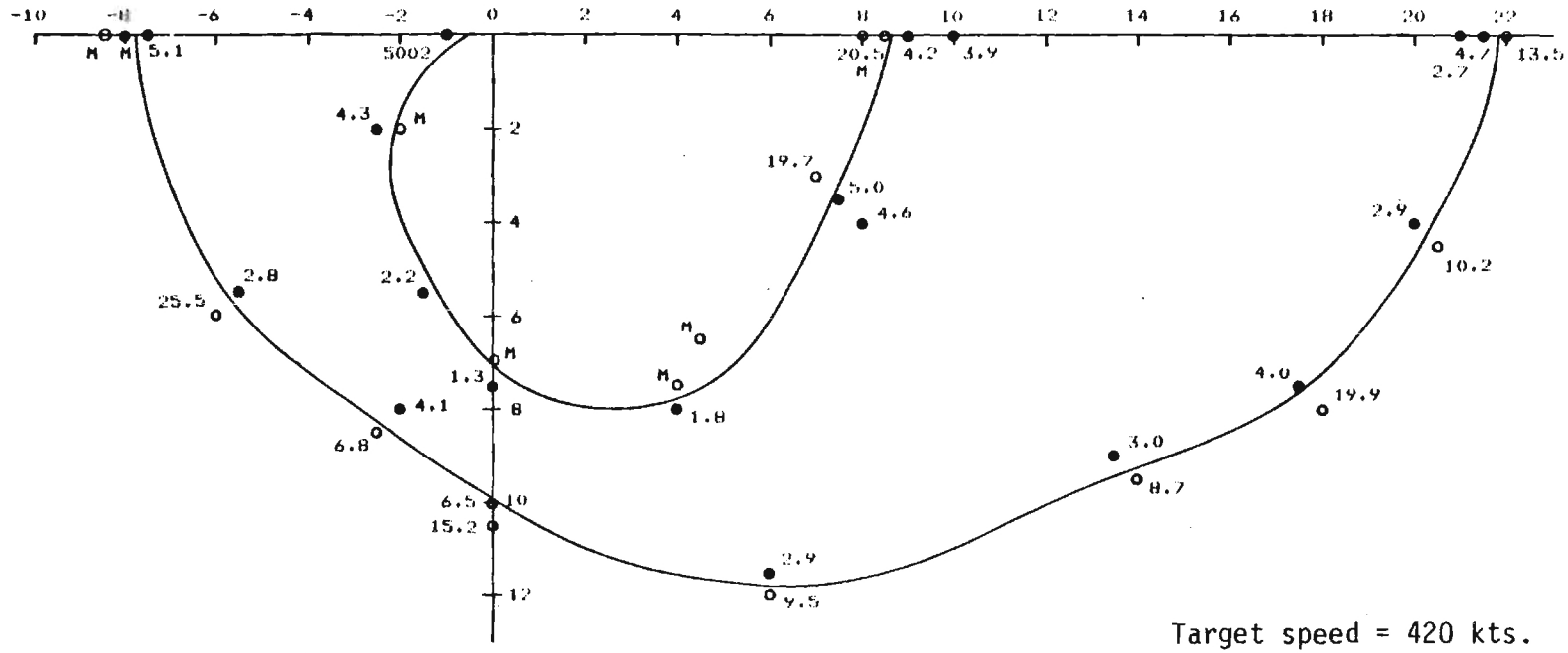

Target speed = 420 kts.

Target altitude = 100 ft.

Each division = 2000 ft.

Figure 7.0-4 Footprint for scenario #4.

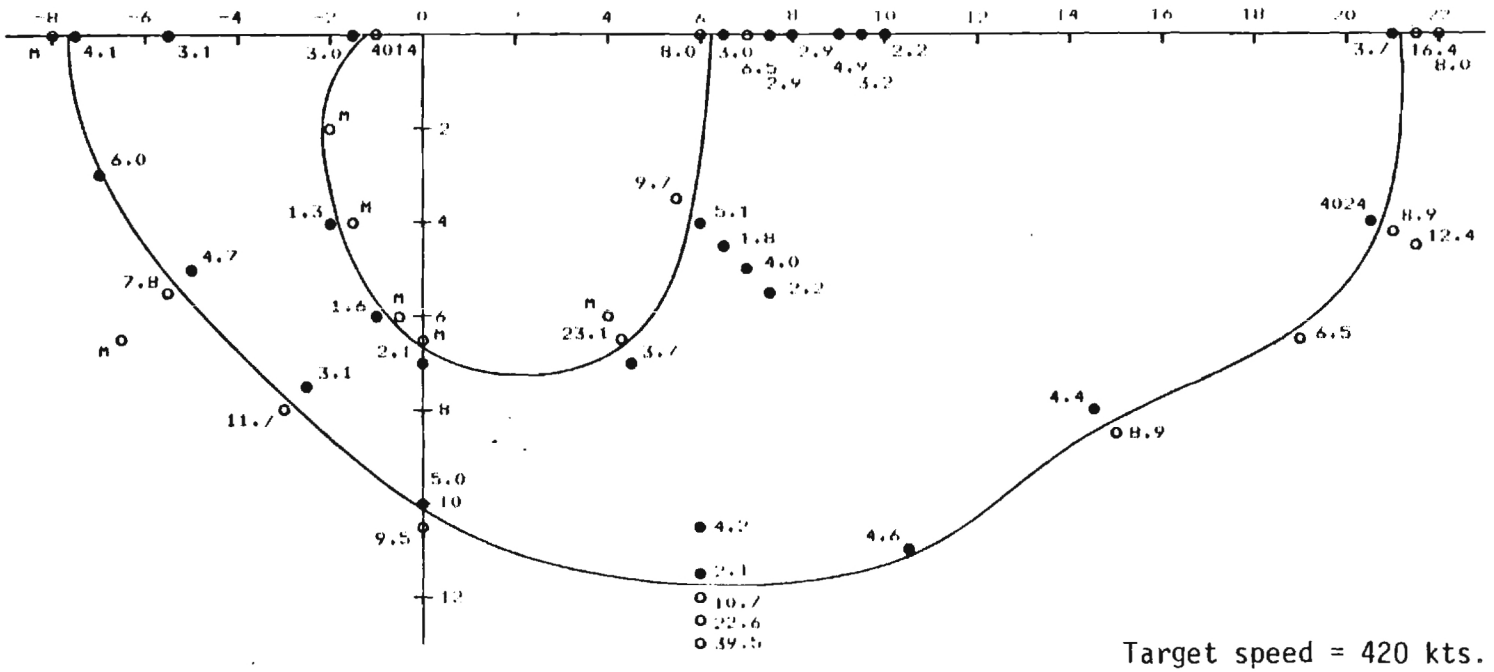

Target speed = 420 kts.
Target altitude = 500 ft.
Each division = 2000 ft.

Figure 7.0-5 Footprint for scenario #5.

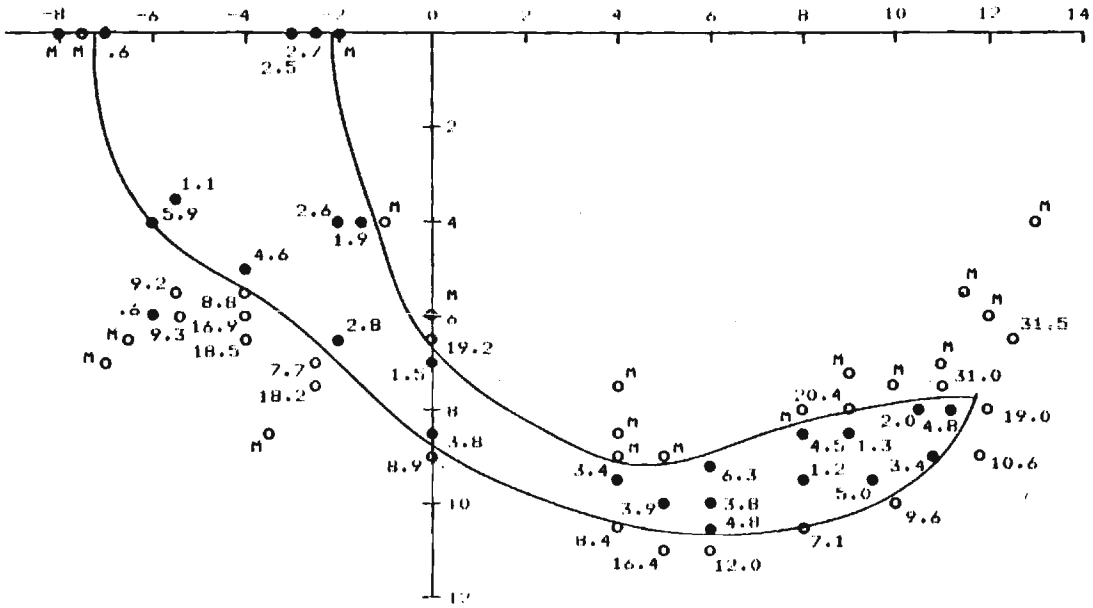

Target speed = 420 kts.
Target altitude = 5000 ft.
Each division = 2000 ft.

Figure 7.0-6 Footprint for scenario #6.

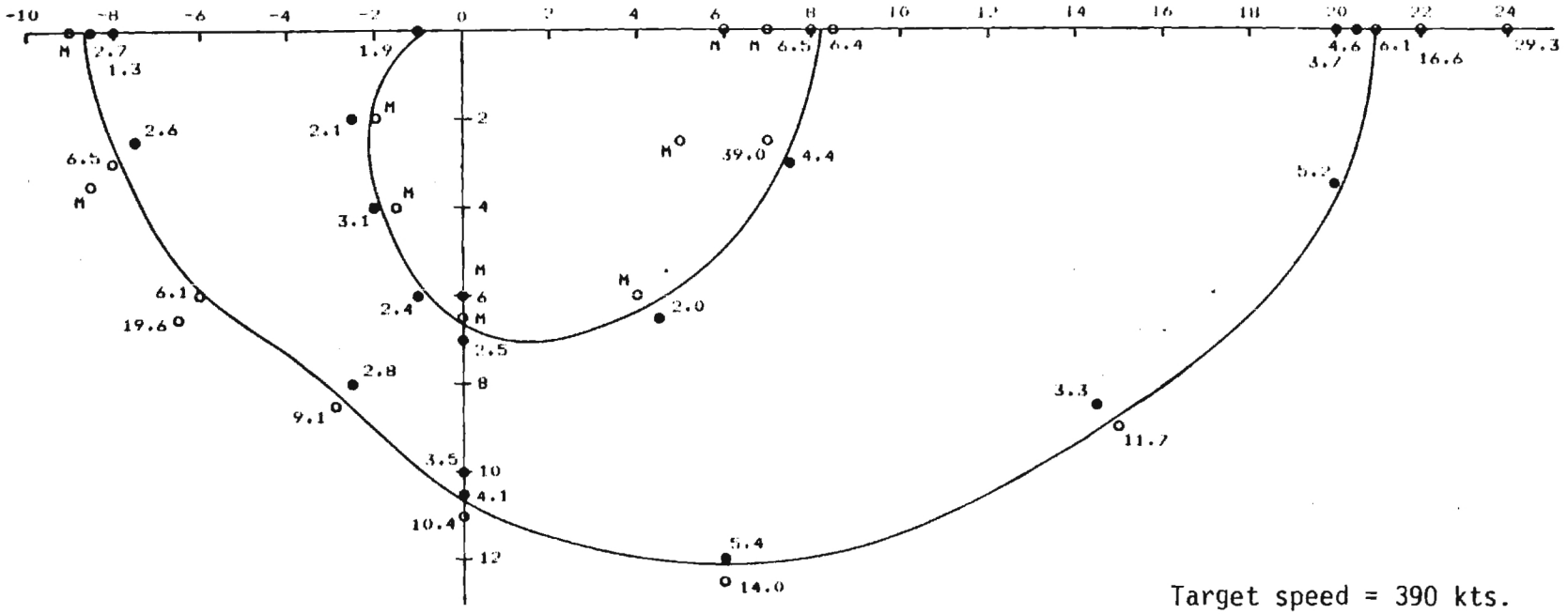

Target speed = 390 kts.
Target altitude = 100 ft.
Each division = 2000 ft.

Figure 7.0-7 Footprint for scenario #7.

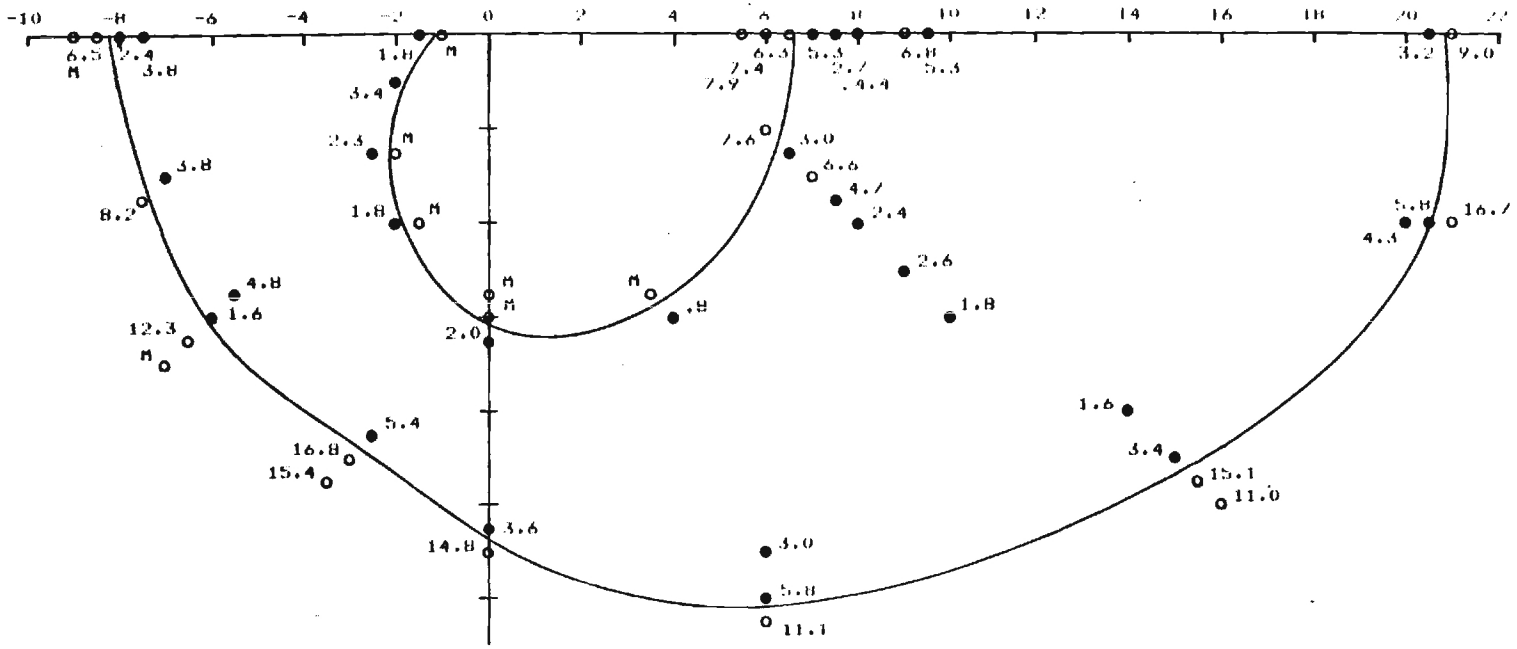

Figure 7.0-8 Footprint for scenario #8.

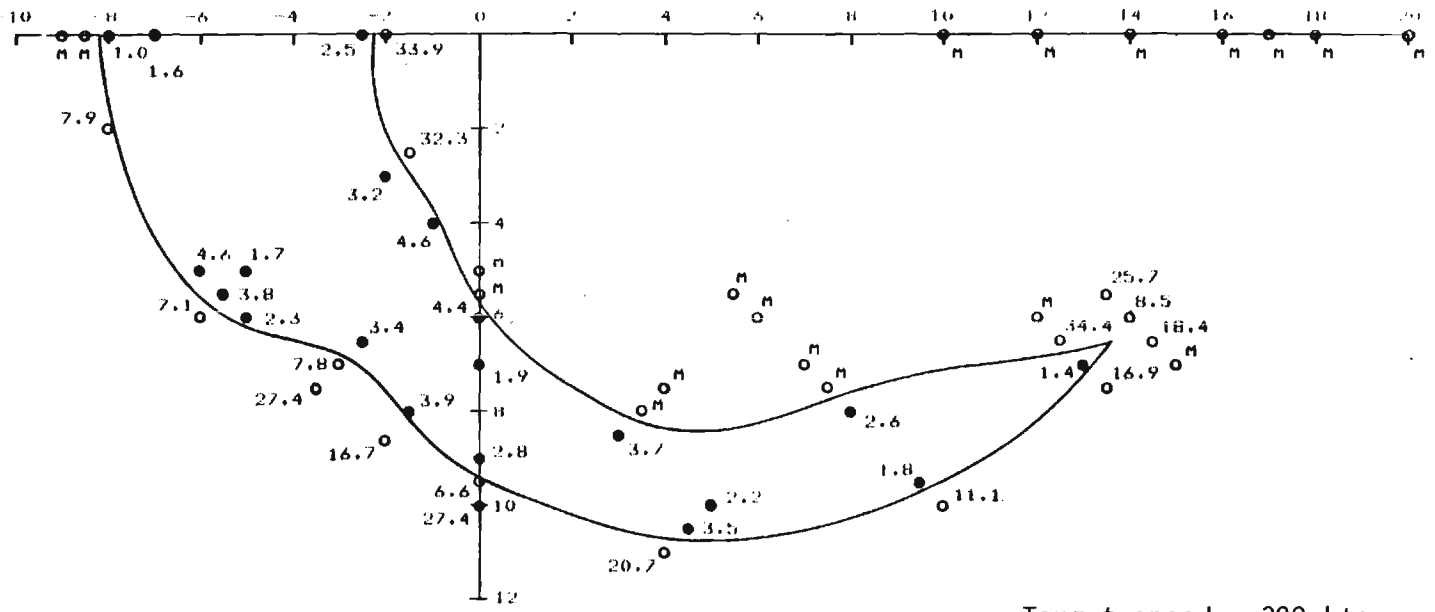

Figure 7.0-9 Footprint for scenario #9.

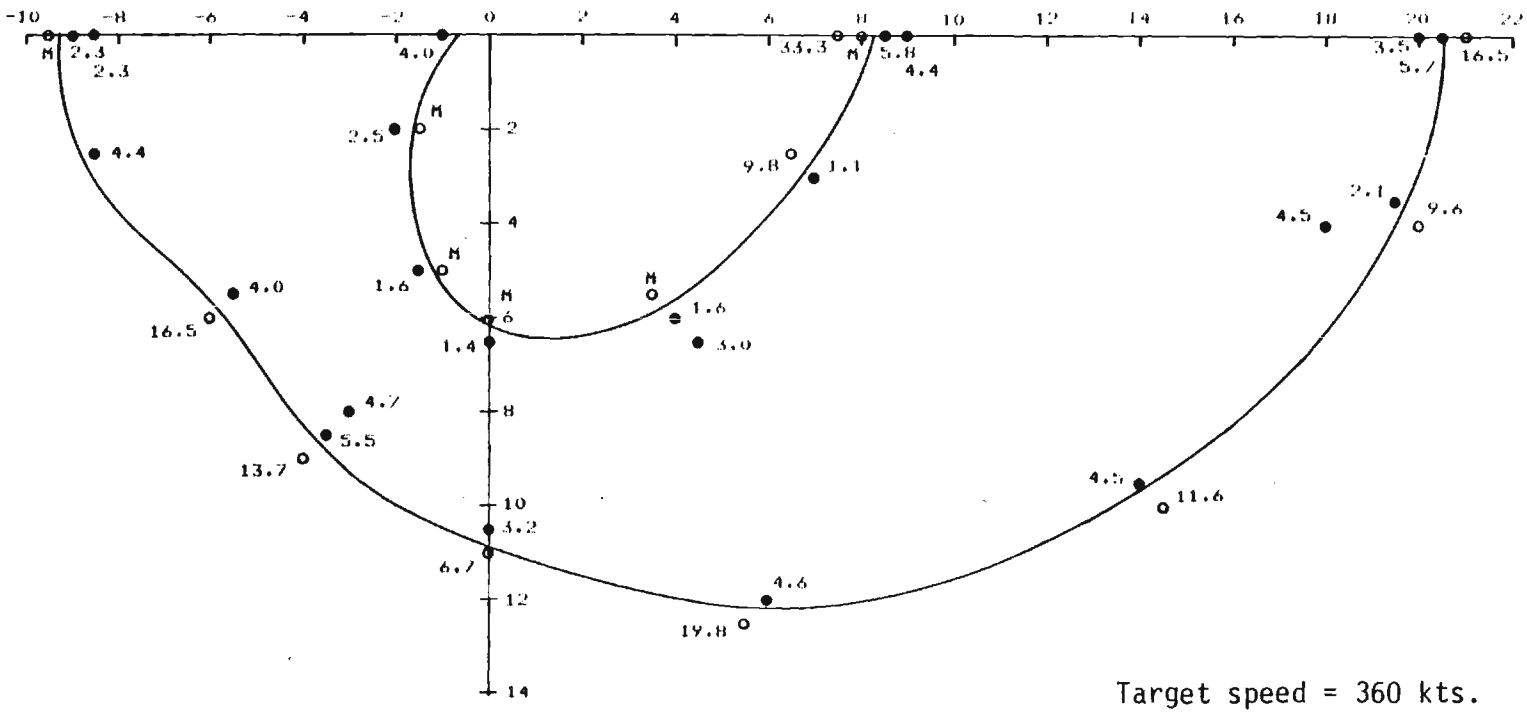

Target speed = 360 kts.
Target altitude = 100 ft.
Each division = 2000 ft.

Figure 7.0-10 Footprint for scenario #10.

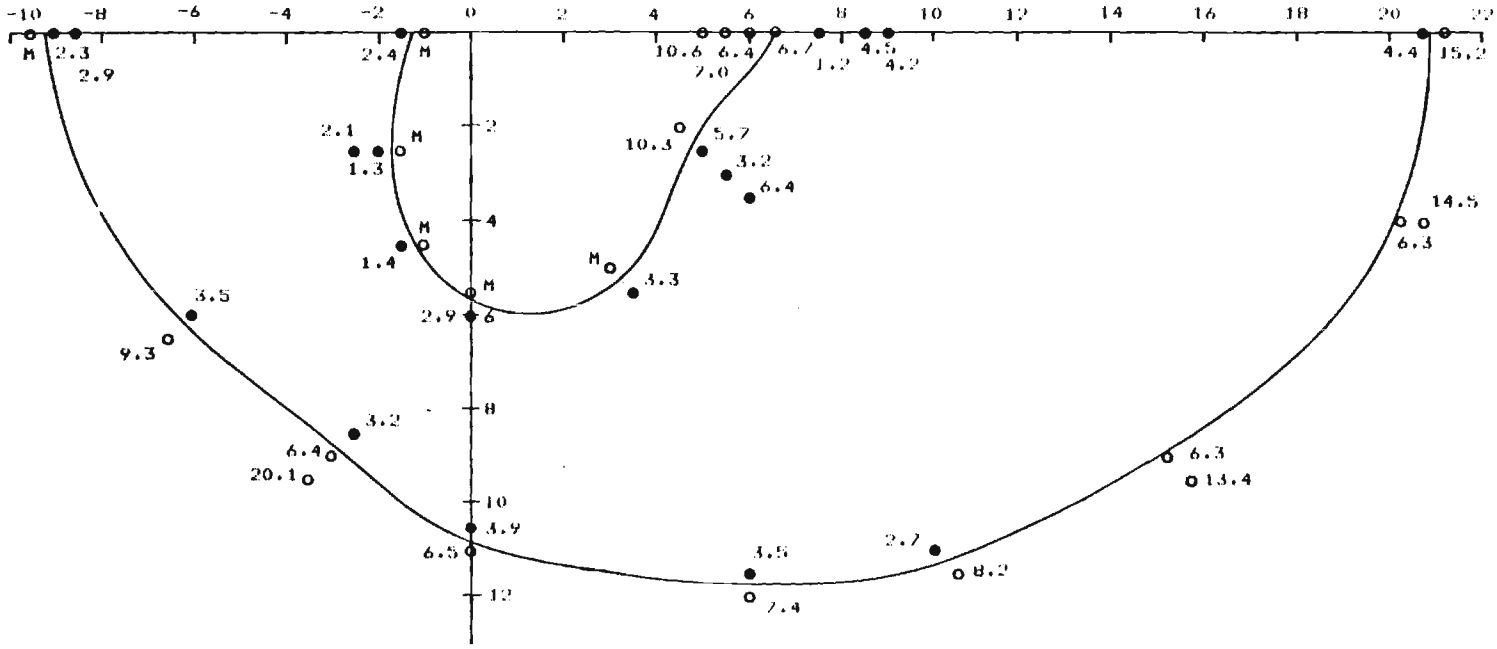

Target speed = 360 kts.
Target altitude = 500 ft.
Each division = 2000 ft.

Figure 7.0-11 Footprint for scenario #11.

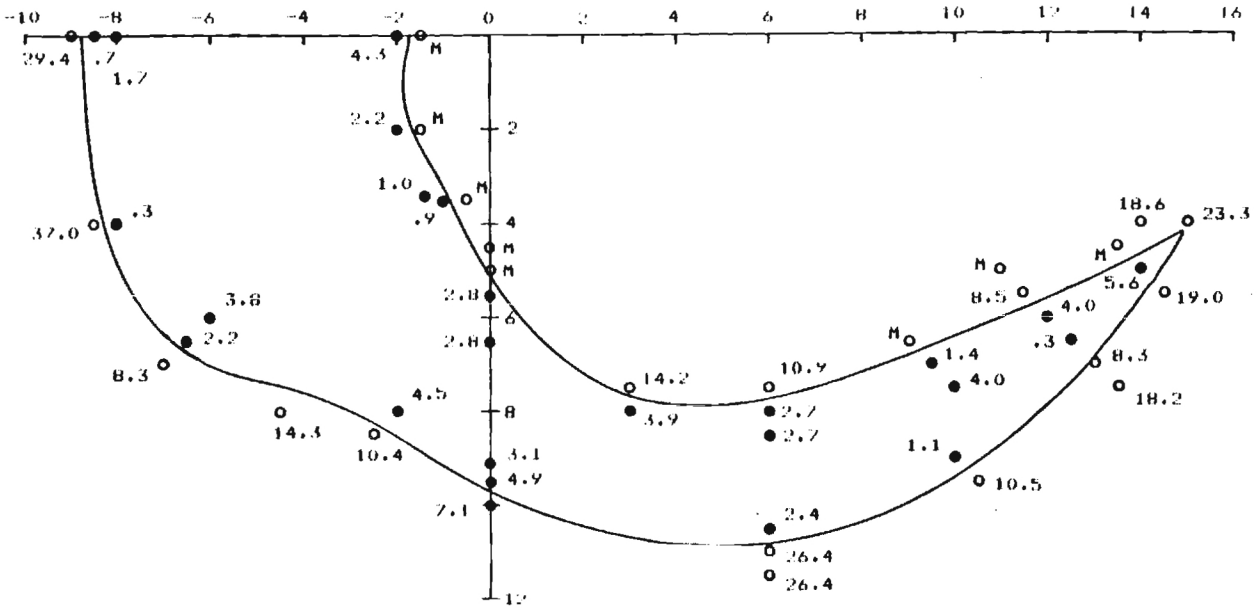

Target speed = 360 kts.
Target altitude = 5000 ft.
Each division = 2000 ft.

Figure 7.0-12 Footprint for scenario #12.

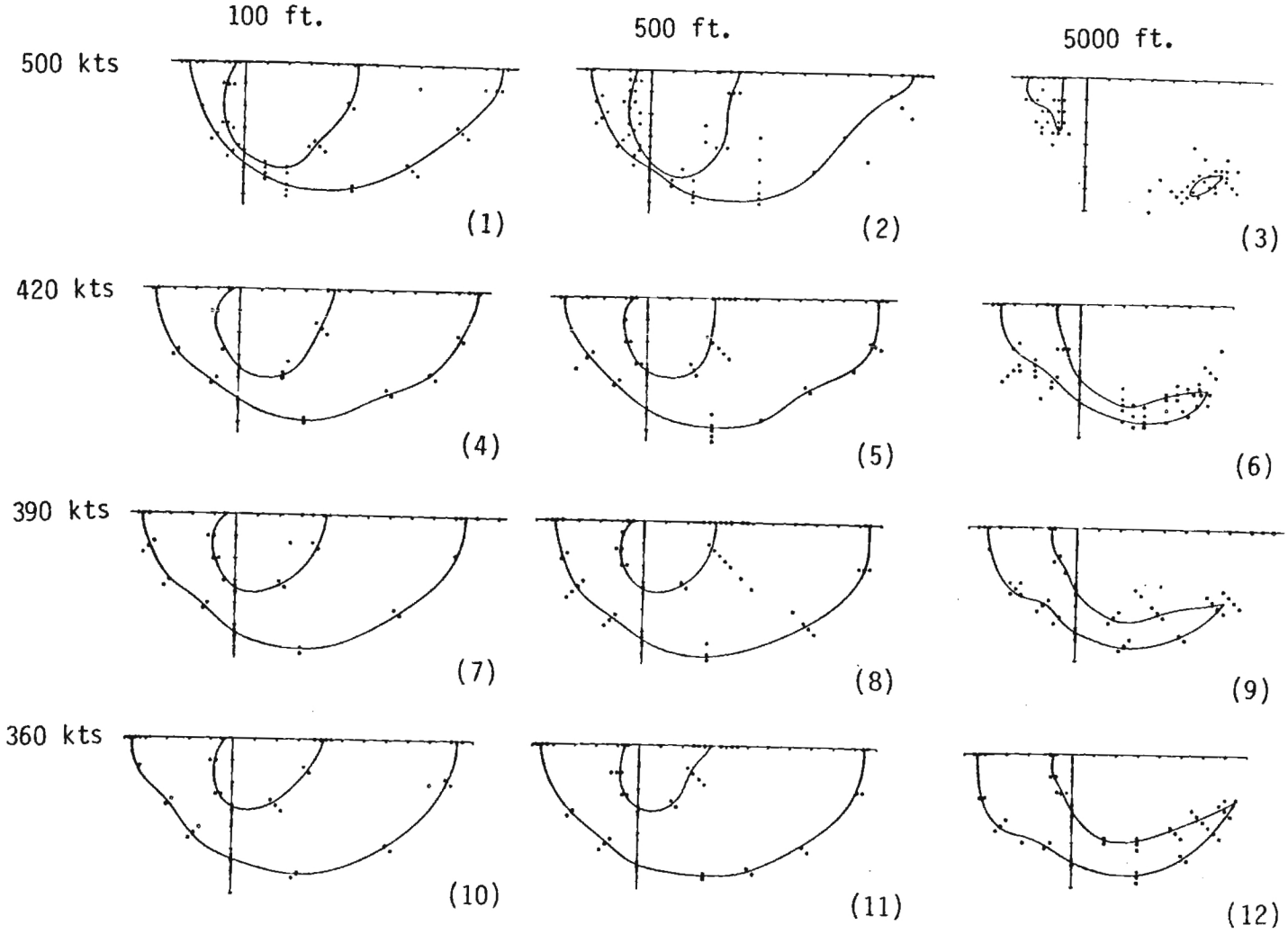

Figure 7.0-13 Footprint summary.

8.0 Anomalies for Multiple Source Targets

In a series of simulations using the DISAMS-1 program involving multiengine aircraft, it was observed that miss distances in some cases were considerably higher than expected and that the magnitude of the miss distances seemed to depend in a rather complicated way on the distance between the engines. To take the simplest case, a two engine aircraft and a missile launch from the tail aspect of the target, if the target speed and altitude are held constant, there seem to be two critical values for engine spacing. For distances larger than the larger of these and for distances smaller than the smaller, miss distances are small and more or less random. As engine spacing increases from the smaller, however, miss distances increase, then decrease again as engine spacing approaches the larger. The following paragraphs are an attempt to examine the cause of this effect.

Consider first a single point source. Energy from the source is focused on the plane of the reticle where it is chopped to encode positional data. This particular reticle , Figure 8.0-1, encodes both radial and angular position of the source image on the reticle plane. Angular position is determined by a phasing sector, radial position by the number of spokes that cross the image, a minimum of six indicating maximum radial distance, a maximum of twelve indicating zero or near zero radial displacement from the origin. For

example, if the reticle is positioned as shown in Figure 8.0-1 at t = 0, the detector output for source images at various positions is shown in Figure 8.0-2.

To generate an error signal which may be used to precess the gyro so that its spin axis points at the target and to maneuver the missile control surfaces so that a proportional navigation path is followed, the seeker electronics processes the detector signal in several stages.

The first of these is the preamplifier and carrier amplifier. This AGC controlled section amplifies and filters the detector signal so that the amplitude of the output is (ideally) constant regardless of the amplitude of the input. The second stage, the demodulator , half wave rectifies the output of the carrier amplifier and produces the envelope of the result. Ideally then, the demodulator output is a series of step functions. Finally, the error signal is generated by extracting from the demodulator output its fundamental, or spin frequency, component. The phase and amplitude of this component reflect the angular and radial position of the source image on the reticle plane.

The set of plots in Figure 8.0-3 show the output of each of these stages for the detector signal shown in Figure 8.0-2a. These are, of course, idealized output. The actual carrier output would show effects of ringing, decay, etc., the demodulator output would not have the sharp shoulders shown, etc. Nevertheless, these signals are the basis on which the seeker performance characteristics are based.

The following paragraphs show how the positional information is extracted from the demodulator signal.

Suppose the period induced by the spin frequency f_s is p, i.e. $p = 1/f_s$ and, for convenience, let $w = 2f_s$. Assuming the source image is held stationary, the demodulator output g(t) can be represented by a Fourier series

$$g(t) = \sum_{n=0}^{\infty} a_n \cos\left(\frac{2n\pi t}{p}\right) + b_n \sin\left(\frac{2n\pi t}{p}\right)$$

$$= \sum_{n=0}^{\infty} a_n \cos(n\omega t) + b_n \sin(n\omega t)$$

For a single source, g(t) will have the form of the step function shown in Figure 8.0-4 for some $0 \leq \alpha \leq \beta \leq 1$. It is possible for the nonzero portion to extend past t = p to the right and/or past t = 0 to the left, but by periodicity it is sufficient to consider the case of $0 \leq \alpha$ and $\beta \leq 1$. The fundamental component of g(t) is the term

$$g_1(t) = a_1 \cos(\omega t) + b_1 \sin(\omega t)$$

so we shall calculate only a_1 and b_1,

$$a_1 = \frac{2}{p} \int_0^p g(s) \cos\left(\frac{2\pi s}{p}\right) ds$$

$$= \frac{A}{\pi} (\sin(2\pi\beta) - \sin(2\pi\alpha))$$

$$b_1 = \frac{2}{p} \int_0^p g(s) \sin\left(\frac{2\pi s}{p}\right) ds$$

$$= -\frac{A}{\pi}(\cos(2\pi\beta) - \cos(2\pi\alpha))$$

The fundamental component then is

$$g_1(t) = \frac{A}{\pi}\left((\sin(2\pi\beta) - \sin(2\pi\alpha))\cos(\omega t) - (\cos(2\pi\beta) - \cos(2\pi\alpha))\sin(\omega t)\right)$$

Recall the identities

$$\sin(A) - \sin(B) = 2\sin\left(\frac{A - B}{2}\right)\cos\left(\frac{A + B}{2}\right)$$

$$\cos(A) - \cos(B) = -2\sin\left(\frac{A + B}{2}\right)\sin\left(\frac{A - B}{2}\right)$$

Then

$$g_1(t) = \frac{2A}{\pi}\left\{\sin\left(2\pi\left(\frac{\beta - \alpha}{2}\right)\right)\cos\left(2\pi\left(\frac{\beta + \alpha}{2}\right)\right)\cos(\omega t) + \sin\left(2\pi\left(\frac{\beta + \alpha}{2}\right)\right)\sin\left(2\pi\left(\frac{\beta - \alpha}{2}\right)\right)\sin(\omega t)\right\}$$

$$= \frac{2A}{\pi}\sin\left(2\pi\left(\frac{\beta - \alpha}{2}\right)\right)\cos\left(\omega t - 2\pi\left(\frac{\beta + \alpha}{2}\right)\right)$$

If a source image is initially at (r,θ), Figure 8.0-5, the reticle must turn $2\pi\alpha$ radians before the chopping sector intersects the image and it must turn $2\pi\beta$ radians for the chopping sector to pass the image. Note that α and β again indicate a fraction of a period and that the α and β here are the same α and β that appear in Figure 8.0-4. We have then

$$2\pi\left(\frac{\alpha + \beta}{2}\right) = 2\pi\left(\frac{\alpha + (2\gamma + \alpha)}{2}\right) = 2\pi(\alpha + \gamma) = \theta$$

Thus the phase of g_1 is the angular coordinate of the

source image.

The equation of the upper half circle which forms part of the boundary between the phasing and chopping sectors is

$$\rho = 2a \sin(\phi) \qquad \pi/2 \leq \phi \leq \pi$$

hence from Figure 8.0-5

$$2\pi\left(\frac{\beta - \alpha}{2}\right) = 2\pi\left(\frac{(2\gamma + \alpha) - \alpha}{2}\right) = 2\pi\gamma$$

$$\doteq \sin^{-1}\left(\frac{\gamma}{2a}\right)$$

So

$$\sin\left(2\pi\left(\frac{\beta - \alpha}{2}\right)\right) = \sin\left(\sin^{-1}\left(\frac{r}{2a}\right)\right) = \frac{r}{2a}$$

Thus, $g_1(t)$ can be written as

$$g_1(t) = \frac{Ar}{\pi a} \cos(\omega t - \theta)$$

where r and θ are the polar coordinates of the source image on the reticle plane.

The last equation shows that the magnitude of $g_1(t)$ is directly proportional to the radial coordinate, r, of the source image. The factor "a" is fixed, but A will vary with the intensity of the source. To eliminate this effect, AGC is employed in the carrier amp so that the amplitude of its output, hence of the demodulator, is independent of source intensity. Ideally, this results in a demodulated signal that has the same maximum over all cycles regardless of the intensity or

number of sources. We shall assume in the sequel that this maximum is unity.

Suppose now that two source images fall on the reticle, one at (r_1,θ_1) with corresponding α_1 and β_1, Figure 8.0-7a, the second at (r_2,θ_2) with corresponding α_2 and β_2 as shown in Figure 8.0-7b. Suppose further that the intensity of the first is A_1 and of the second, A_2. The AGC then makes the effective intensity of the first source $a_1 = A_1/(A_1 + A_2)$ and of the second $a_2 = A_2/(A_1 + A_2)$. Figure 8.0-7c shows the detector signal, Figure 8.0-7d the carrier amp output, and Figure 8.0-7e the demodulated signal. The fundamental component of Figure 8.0-7e, which is shown as Figure 8.0-7f, is given by

$$g_1(t) = \frac{a_1 r_1}{a\pi}\cos(\omega t - \theta_1) + \frac{a_2 r_2}{a\pi}\,\mathrm{cso}(\omega t - \theta_2)$$

$$= \frac{a_1 r_1}{a\pi}\left[\cos(\omega t)\cos(\theta_1) + \sin(\omega t)\sin(\theta_1)\right] +$$

$$\frac{a_2 r_2}{a\pi}\left[\cos(\omega t)\cos(\theta_2) + \sin(\omega t)\sin(\theta_2)\right]$$

$$= \frac{1}{a\pi}((a_1 r_1\cos(\theta_1) + a_2 r_2\cos(\theta_2))\cos(\omega t) +$$

$$(a_1 r_1\sin(\theta_1) + a_2 r_2\sin(\theta_2))\sin(\omega t))$$

Let

$$B = a_1 r_1\cos(\theta_1) + a_2 r_2\cos(\theta_2),$$
$$C = a_1 r_1\sin(\theta_1) + a_2 r_2\sin(\theta_2),$$

and

$$D = \sqrt{B^2 + C^2}$$

Then write g_1 as

$$g_1(t) = \frac{D}{a\pi}\left(\frac{B}{D}\cos(\omega t) + \frac{C}{D}\sin(\omega t)\right)$$

Since $(B/D)^2 + (C/D)^2 = 1$, there is a μ so that $\cos(\mu) = B/D$ and $\sin(\mu) = C/D$, hence

$$g_1(t) = \frac{D}{a\pi}\cos(\omega t - \mu)$$

Now

$$D^2 = (a_1 r_1 \cos(\theta_1) + a_2 r_2 \cos(\theta_2))^2 + (a_1 r_1 \sin(\theta_1) + a_2 r_2 \sin(\theta_2))^2$$

$$= (a_1 r_1)^2 + (a_2 r_2)^2 + 2(a_1 r_1)(a_2 r_2)\cos(\theta_2 - \theta_1)$$

D then is the length of the major diagonal of the parallelogram of Figure 8.0-8. Observe that the line segment FG has the length of

$$a_1 r_1 \sin(\theta_1) + a_2 r_2 \sin(\theta_1)$$

and line segment OF has length of

$$a_1 r_1 \cos(\theta_1) + a_2 r_2 \cos(\theta_2).$$

Thus μ is the angle the major diagonal makes with the x-axis. The point (D,μ), Figure 8.0-9, then is the point G. If $a_1 = a_2 = 1/2$, (D,μ) is the point of intersection of the major and minor axes of the parallelogram with vertices at $(0,0)$, (r_1,θ_1), and (r_2,θ_2). The expression

$$g_1(t) = \frac{D}{a\pi} \cos(\omega t - \mu)$$

which resulted from two sources is, therefore, the same as that of a single source at the centroid of the two. Note that the effect of a_1 and a_2 is to make this an energy centroid for sources of unequal strength rather than a geometric centroid. Note: a simple proof that (D,μ) lies on the minor diagonal of the large parallelogram of Figure 8.0-9 is to express (D,μ) in rectangular coordinates and show that the point coordinates satisfy the equation of the line between (r_1,θ_1) and (r_2,θ_2).

The case just considered is more special than has been indicated. This is because the spacing of the two source images was selected so that the resulting signals tended to reinforce each other, i.e., for the most part both images entered and exited transparent regions at the same time. This is the case, for example, if the source images are at A and B on Figure 8.0-7 and result in an error signal with 0^o phase. Suppose now the images are at C and D. One would expect an error signal again with a 0^o phase. Examination of Figure 8.0-6 shows however that as one image enters an opaque region, the other enters a transparent one. The resulting signals are shown in Figure 8.0-10. It is clear from the demodulator signal that the error signal will be almost 180^o out of phase relative to the A, B error signal, that is, the missile will be guided away from the target. Output from the DISAMS-1 seeker model, Figure 8.0-11, shows the various signals as two point sources are separated symmetrically from the reticle

axis ($\theta = 0$). Note that the 100Hz. error signal should keep a fixed 0^{o} phase if proper tracking is to occur. In fact, the phase varies by 180^{o}. In this special simulation, the error signal was not allowed to precess the gyro. In some flight simulations, however, the seeker appears to track a point below the two source target, and that track point varies as the missile closes. This, of course, results in large miss distances.

It was mentioned earlier that if the engines are widely separated or very close, the above effect does not seem to seriously affect miss distance. A rational for this is the following. If the engines are widely separated, one will go out of the field of view sufficiently early in the simulation for the missile to correct its path and impact the target. If the engines are close, the missile will be so close to the target before the effect is serious that the erroneous error signals will not change the path by much. The values of these critical engine distances depend on several factors such as the aspect angle between target and missile, closing speed, etc. Another factor, which has not been explored, is the degradation of the detector signal resulting from the image size growing as the missile closes. It seem unlikely, however, that this effect would be helpful to proper guidance.

This brief study is not conclusive. It is not known how serious this effect is in actual flights. It has been reported, however, that the missile sometimes oscillates during the end game against multiengine targets. This has commonly been attributed to the seeker oscillating between the two or more sources.

That oscillation has not been observed during simulations using DISAMS-1, but it may be due to the effect just described.

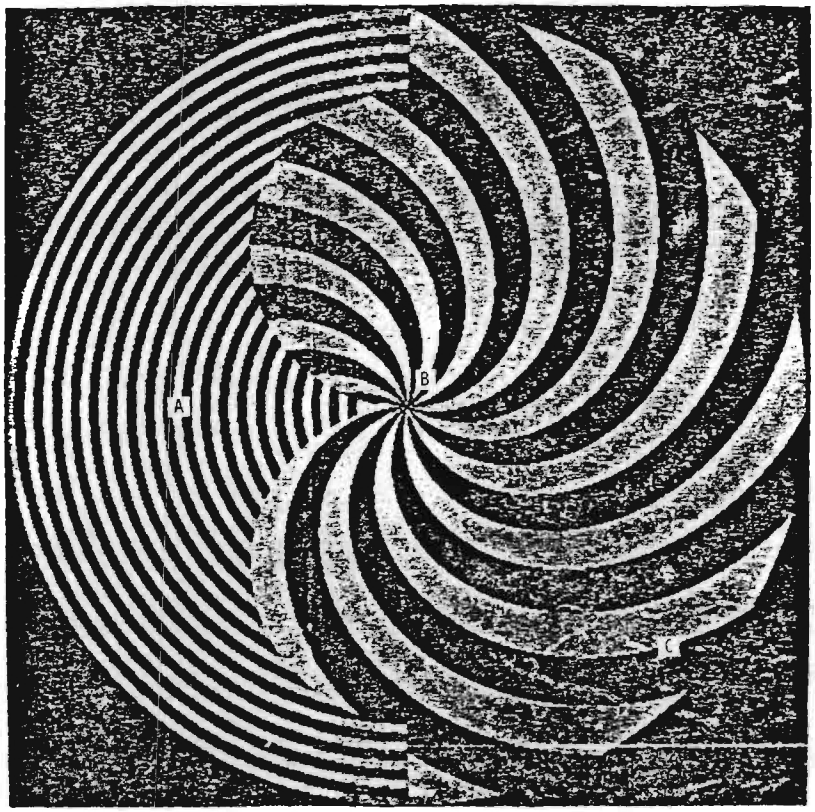

Figure 8.0-1 Source positions on the reticle at t = 0.

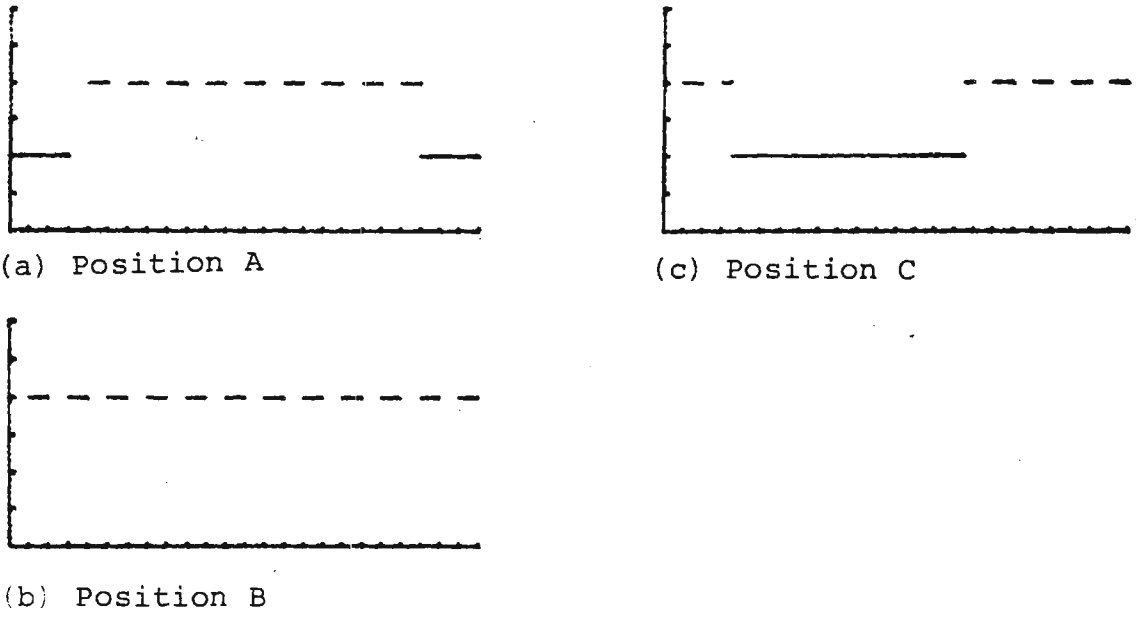

Figure 8.0-2 Detector output for source positions on Figure 8.0-1.

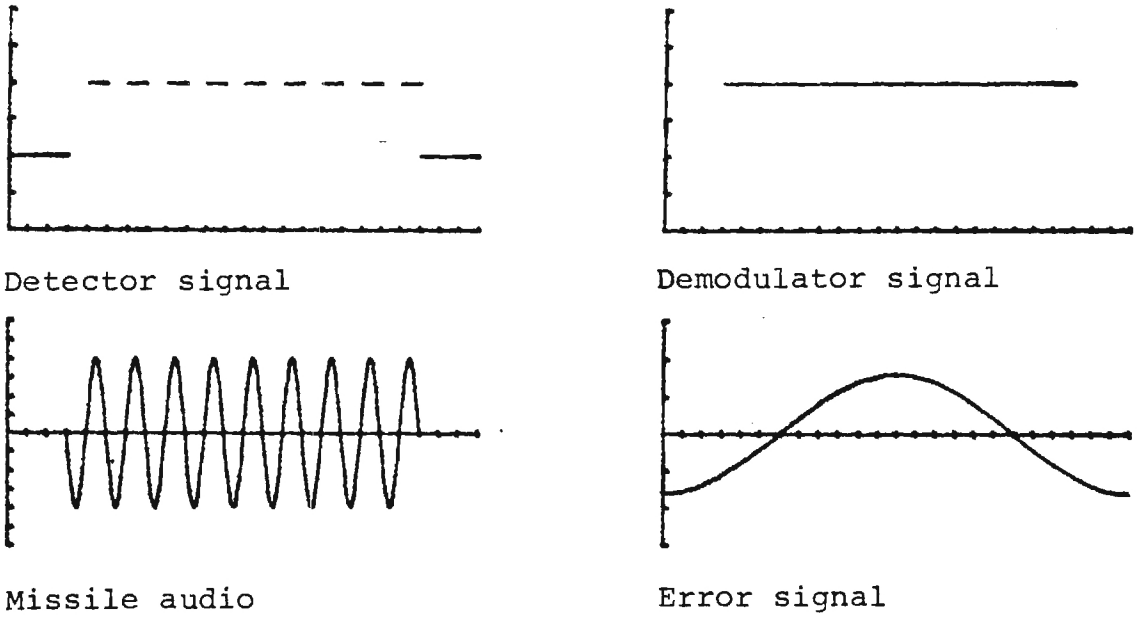

Figure 8.0-3 Detector signal and resulting seeker output.

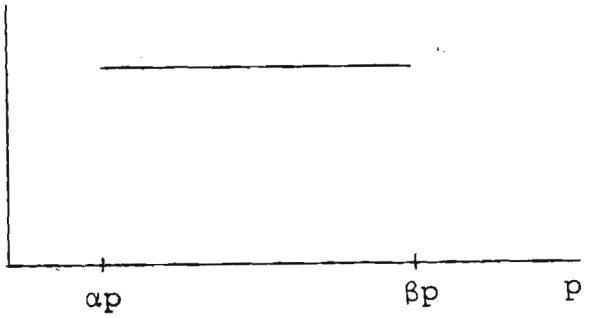

Figure 8.0-4 Demodulator signal.

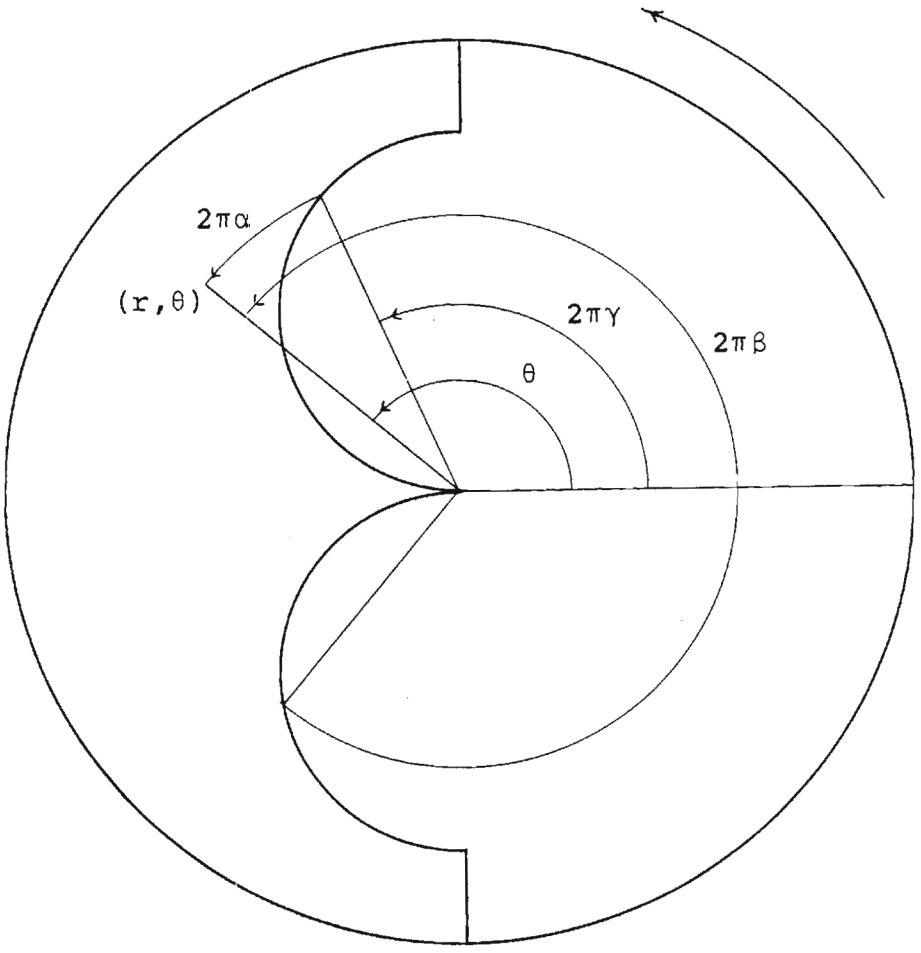

Figure 8.0-5 Image position geometry.

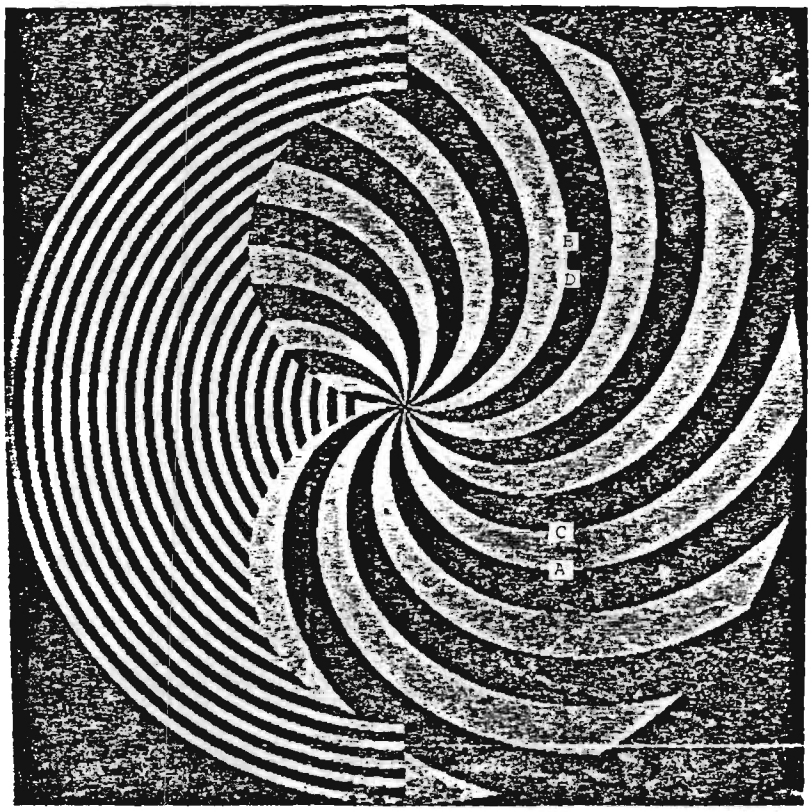

Figure 8.0-6 Two source target image positions.

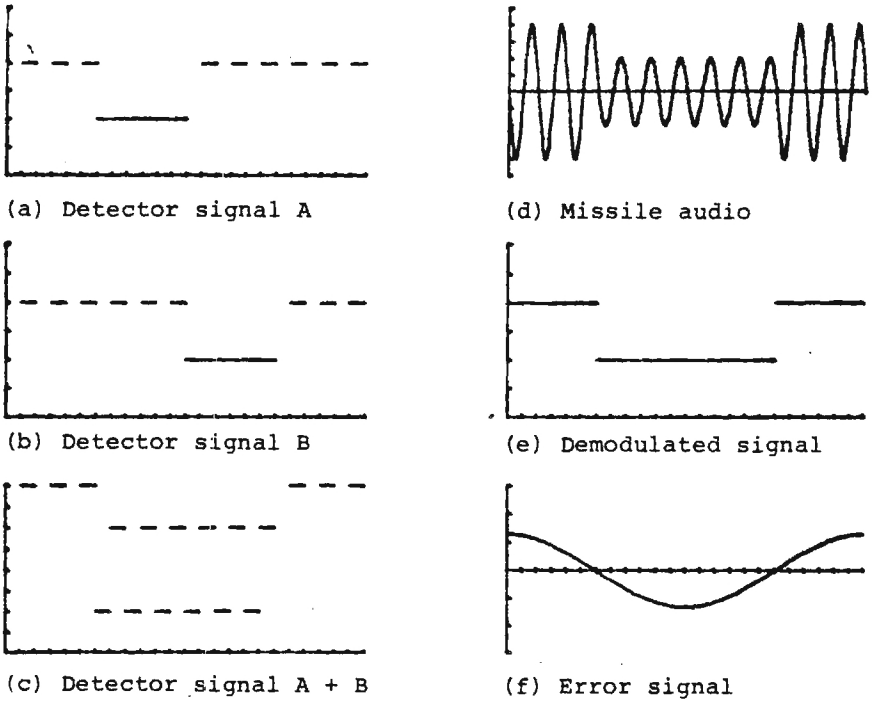

Figure 8.0-7 Detector and seeker signals for positions A,B of Figure 8.0-6.

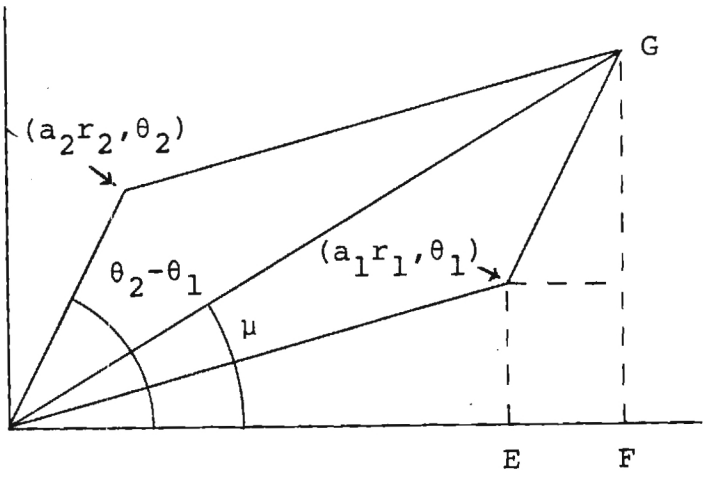

Figure 8.0-8 Source position - error signal relations.

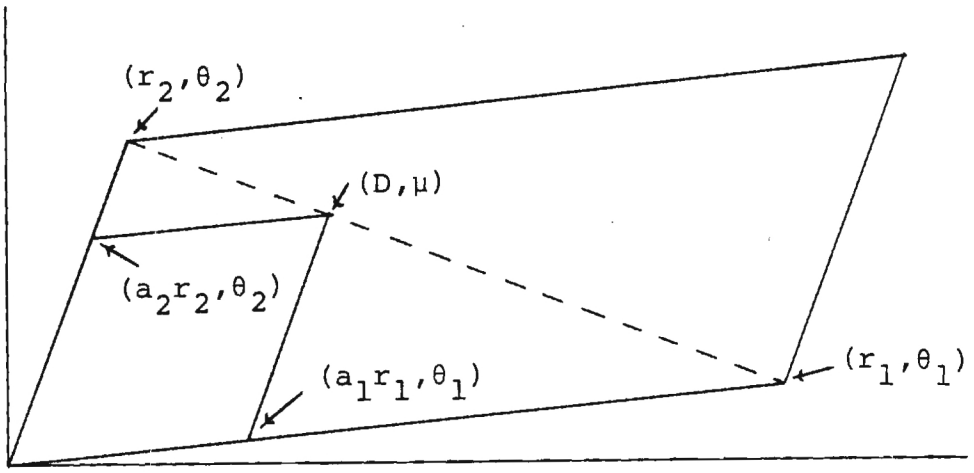

Figure 8.0-9 Centroid relations.

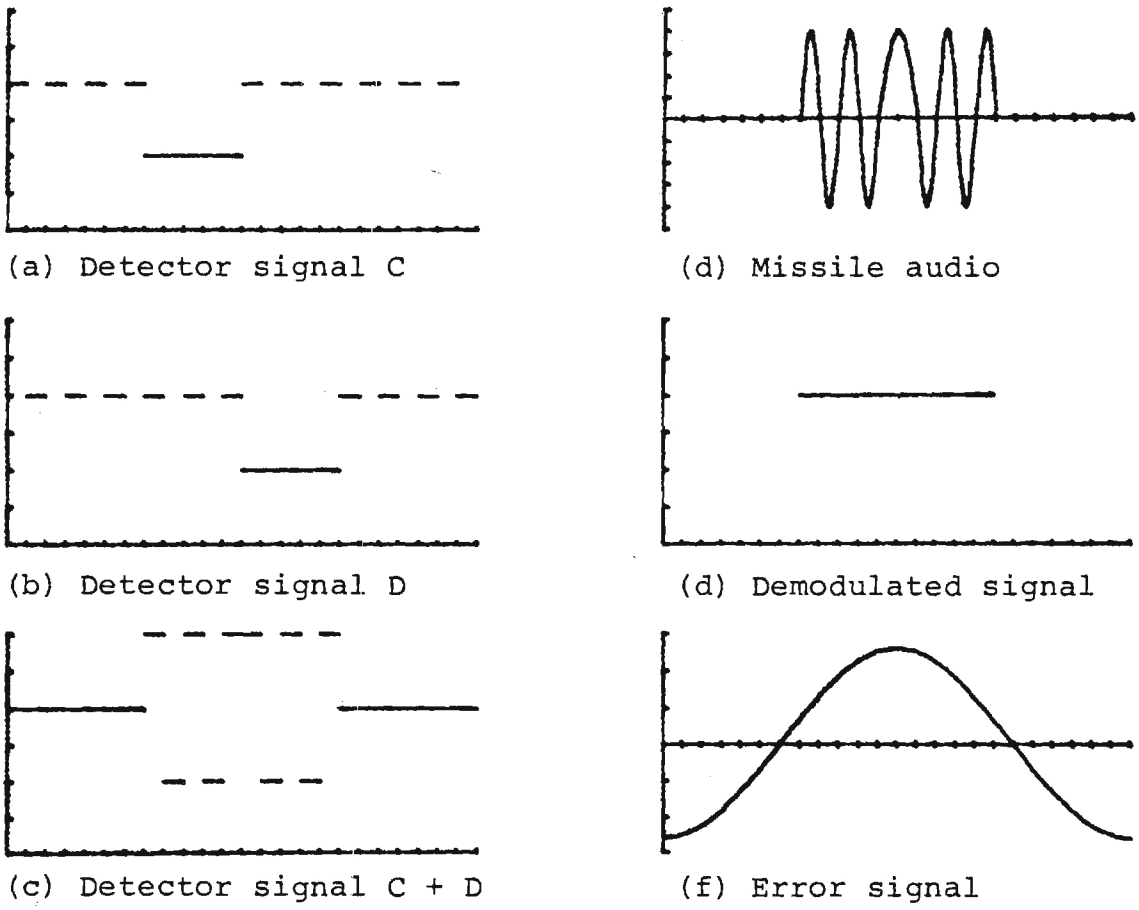

Figure 8.0-10 Detector and seeker signals for positions C,D of Figure 8.0-6.

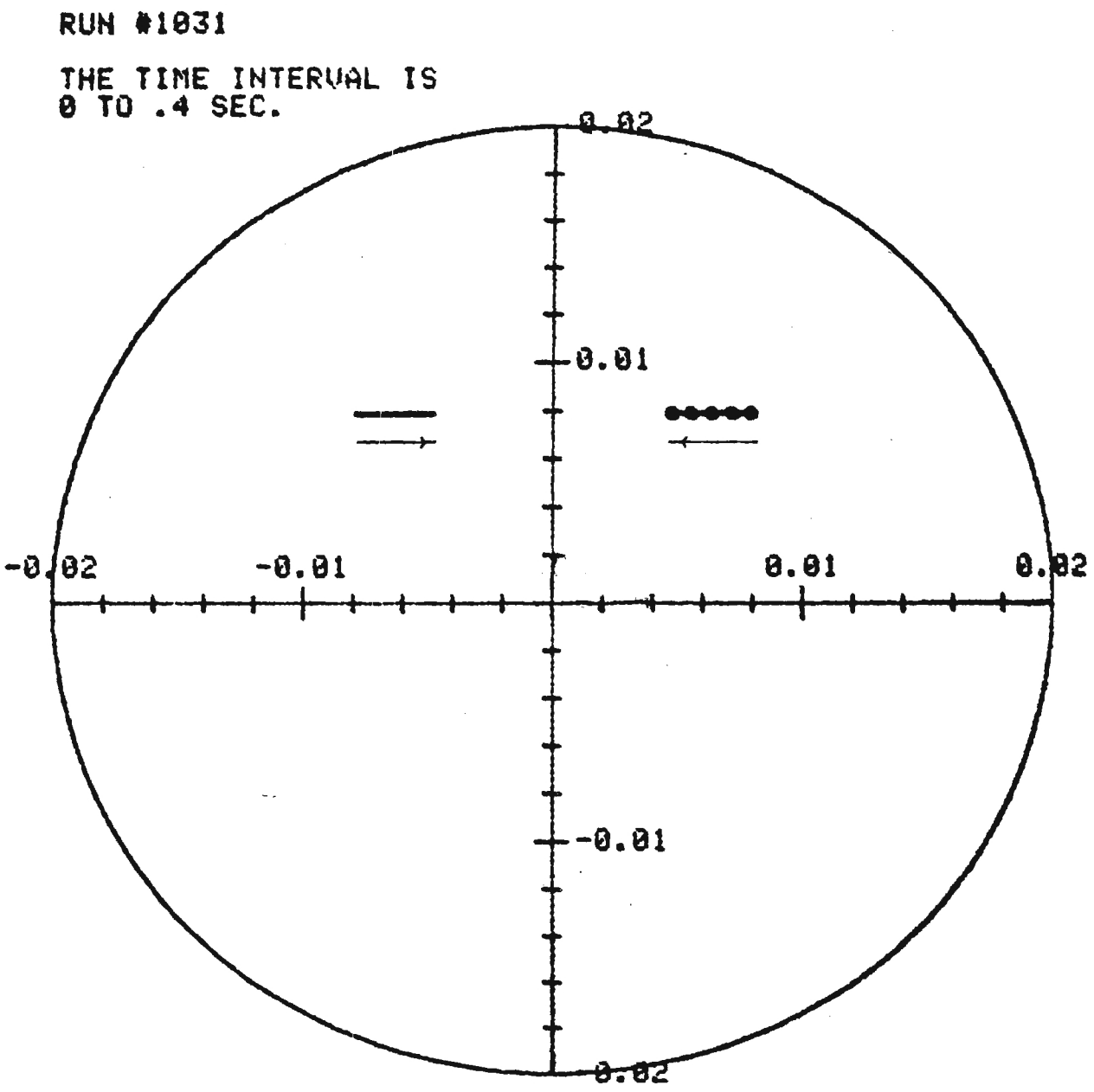

Figure 8.0-11(a) Source positions on the reticle

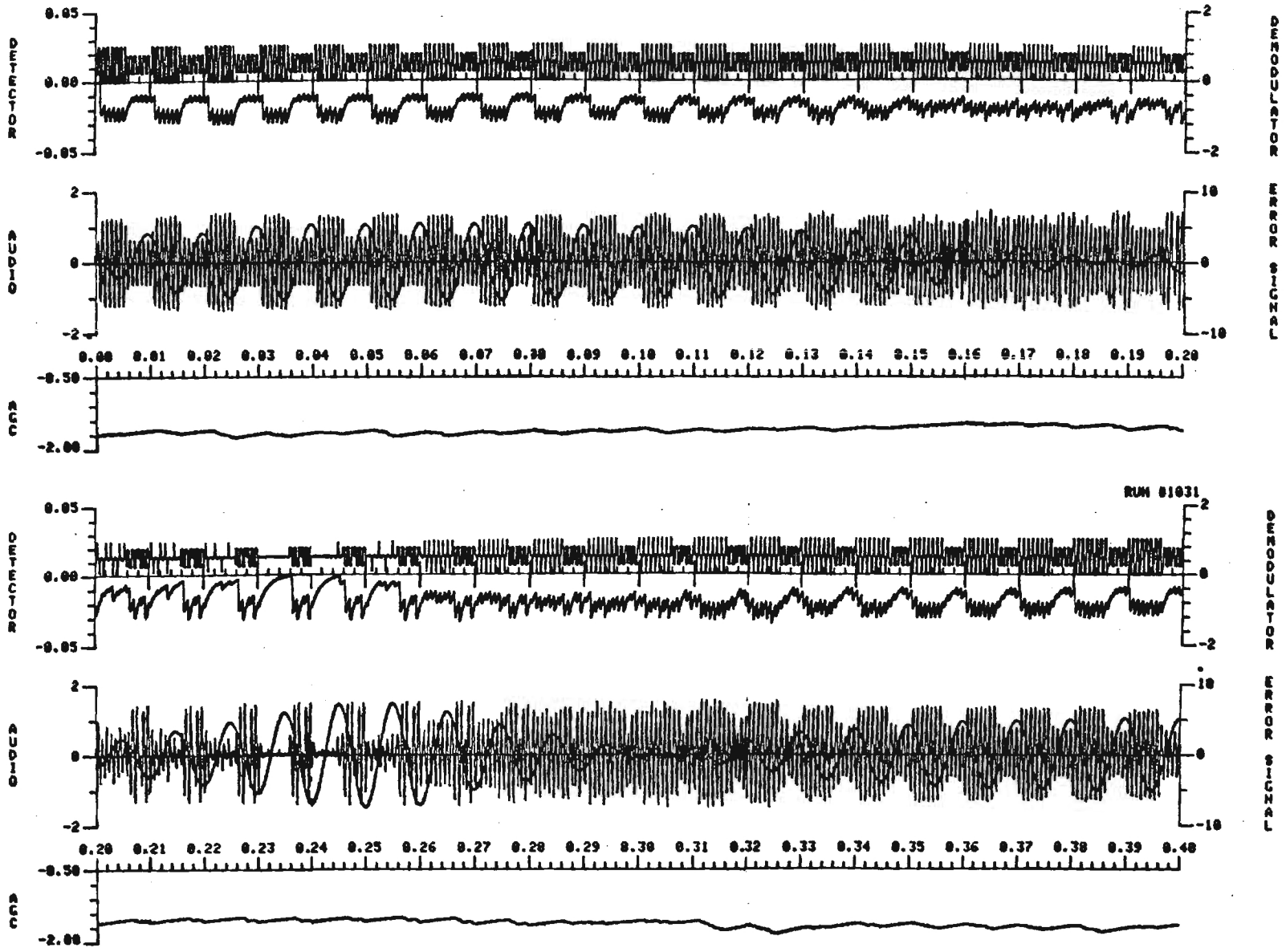

Figure 8.0-11(b) Phase change in the error signal

REFERENCES

(1) Mullikin, A. L., Loefer, G. R. and Weathersby, M. R. "An Infrared Missile 6-DOF Model," Final Report A-2438. Engineering Experiment Station, Ga. Inst. of Tech., Atlanta, Ga., May 1983. (Confidential)

(2) TR-ML82-MICOM-0107 A-34, Vol I (Introduction through Appendix E) and Vol. II (Appendix F through Conclusions), August 1982. (Confidential)